J. Fluid Mech. (1997), *vol.* 346, *pp.* 201–237. Printed in the United Kingdom

© 1997 Cambridge University Press

Ensemble-averaged measurements in the turbulent near wake of two side-by-side square cylinders

By V. KOLÁŘ[1], D. A. LYN[2] AND W. RODI[3]

[1]Institute of Hydrodynamics, Academy of Sciences, Podbabská 13, 166 12 Prague 6, Czech Republic

[2]School of Civil Engineering, Purdue University, W. Lafayette, IN47907, USA

[3]Institute for Hydromechanics, Universität Karlsruhe, 76128 Karlsruhe, Germany

(Received 29 July 1996 and in revised form 21 April 1997)

The ensemble-averaged characteristics of the turbulent near-wake flow around two side-by-side identical square cylinders at a Reynolds number $\approx 23\,100$ have been studied using a two-component laser-Doppler velocimeter system. The work focuses on a single case with a gap/diameter ratio of 2, for which the resulting individual vortex streets are coupled so as to yield a flow predominantly symmetric about the line midway between the two cylinders. Data sorting or conditioning according to phase was performed with the aid of pressure signals taken from taps on a sidewall of each cylinder. The two-cylinder results are compared in detail to results from a previous study of the one-cylinder case. Vortex structures shed on the side towards the flow centreline, termed inner structures, are distinguished from those shed on the free-stream side, termed outer structures, and the differences between the features associated with the two different structures are examined. The circulation associated with outer structures evolves downstream in a manner similar to that observed in the one-cylinder case, but the circulation of the inner structures is found to decrease dramatically downstream. This not only gives support to previous theoretical predictions but also reconciles these with previously apparently conflicting experimental observations. Information regarding vortex structure motion and the relevant length and time scales is obtained. Differences between momentum and vorticity transport, particularly across the flow centreline are pointed out, and effective turbulent vorticity fluxes are defined. Similarities in local flow topologies in one- and two-cylinder cases are discussed, and the role of local velocity-gradient invariants and their relationship to critical points and turbulence statistics are examined.

1. Introduction

The turbulent flow around a single two-dimensional bluff body, whether a circular (e.g. Cantwell & Coles 1983) or square cylinder (e.g. Lyn *et al.* 1995, hereafter referred to as LERP) or bluff plate (e.g. Kiya & Matsumara 1988) has received much recent attention, and insight has been gained into the features of the near-wake turbulent flow. Nevertheless, the focus on single-body wake flows may yield a narrow and overly simple picture. As an extension of earlier studies of single-bluff-body flows (Lyn & Rodi 1994; LERP), the present work examines experimentally the flow around two identical square-section cylinders, positioned side by side, normal

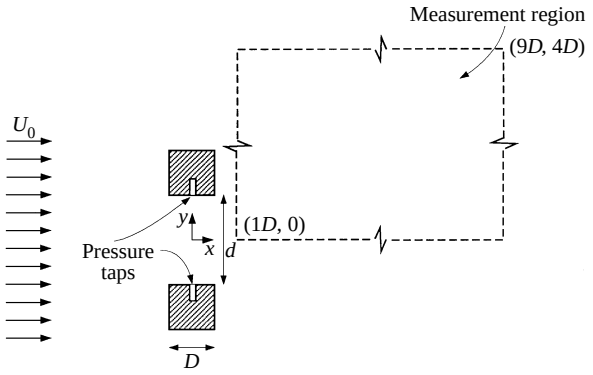

FIGURE 1. Definition sketch of uniform approach flow around two identical side-by-side square-sectioned cylinders

to the approach flow (see figure 1 for a definition sketch). In this type of flow, two distinct vortex streets develop for a range of conditions depending on the separation between the bodies. If the bodies are sufficiently close, the two vortex streets interact strongly, and flow features appear that differ significantly from those of a single vortex street behind an isolated bluff body. A study of these features will therefore yield further information about vortex structures and their mutual interaction.

The basic conceptual model which informs this study has been assumed in several previous investigations of single-body flows, such as Cantwell & Coles (1983) and LERP, namely that of a self-sustained quasi-periodic predominantly two-dimensional large-scale flow, the central features of which are the formation, the shedding, and the transport of vortex structures. The (quasi-) periodicity permits a meaningful definition of ensemble averages at constant phase, or, more simply, phase averages. A statistical characterization of the random (or incoherent or turbulent or residual) small-scale motions is then made, in the hope (also implicit in large-eddy simulations) that these motions are more easily modelled or possess a more universal structure. Previous work on single-body flows has focused on the 'equilibrium' region where the already shed vortex structures are convected downstream, with little direct interaction between the different structures. The flow around two bluff bodies differs in this regard, since, even in this region, significant mixing between vortex structures of differently signed vorticities seems to occur, such that some structure characteristics vary strongly with downstream distance.

The bulk of the present work consists of laser-Doppler velocity measurements of turbulent flow around two side-by-side square cylinders for a single gap distance at a single Reynolds number, Re. With some notable modifications, the experimental approach is similar to that used by LERP. Previous experimental work on similar flow configurations has been restricted to flow visualization and/or force (pressure) and/or frequency measurements; the authors are unaware of any other detailed study of the velocity field. The results are discussed with reference to previously proposed hypotheses based on theoretical models as well as the limited force and frequency measurements. The availability of recent velocity measurements of flow around a single square cylinder under approximately the same flow conditions (LERP) also allows a detailed comparison of the two flows to be made, therefore highlighting the features associated with the interaction between vortex streets.

2. Background, review, and scope of the present work

The overwhelming majority of previous studies have been performed with circular cylinders, and so, unless otherwise specifically noted, it should be assumed in the following review that a study was conducted with circular cylinders. With the introduction of another identical bluff body into the flow, a further length scale, the gap separation, d, becomes relevant. In the case of the circular or square cylinder, which can be characterized by a diameter, D, a non-dimensional relative gap distance may be defined, $g^* = d/D$. A number of different flow regimes depending on the value of g^* have been identified (see the review of Zdravkovich 1977). Observations are expected to hold at least qualitatively and possibly crudely quantitatively for square cylinders and other symmetric bluff bodies. For large $g^* \gg 1$, the vortex streets act independently of each other; for $g^* = O(1)$, however, interaction between vortex streets is observed. For $0.5 < g^* < 1$, a biased-flow regime occurs in which an asymmetric (about the centreline) flow pattern develops, as the gap flow is deflected towards one or the other cylinder. The bias may switch from one side to the other in a random fashion. The resulting wake flow has been variously described as 'confused', with wide and narrow wakes, poorly developed vortex streets, and exhibiting two dominant frequencies (Landweber 1942; Bearman & Wadcock 1973). From two-point correlations of hot-wire measurements, Kim & Durbin (1988) inferred that the convection velocity of the shed vortex structures in both wide and narrow wakes was approximately 80% of the free-stream velocity.

A coupled regime in which two distinct well-developed vortex streets are locked into a definite phase relationship is typically observed when $1 < g^* < 5$. Two different modes have been observed in the coupled regime, an in-phase and an in-antiphase mode (see figure 2 for a schematic diagram of the various modes). Williamson (1985) showed, in flow visualization studies at Reynolds number $Re = 100$–200, that the in-phase vortex street eventually merged downstream to form a single wake, and that only the in-antiphase streets remained distinct farther downstream. In the coupled regime, which is the main subject of the present work, the dominant frequency (or Strouhal number, St) has generally been found to be essentially the same as in the single-body case, although Landweber (1942) reported a larger St in experiments with the two-cylinder case. Other time-averaged characteristics are however affected by the presence of the additional body (Bearman & Wadcock 1973). The base pressure coefficient, $\overline{C_{pb}}^t$, becomes more negative, attaining an extremum at $g^* \approx 1.2$. As a consequence, the drag coefficient, $\overline{C}_D^t$, is increased by $\approx 10\%$ (the t-superscript with an overline is used here to denote a long-time average). In addition, a repulsive lift force is measured.

The stability of coupled vortex streets was analysed by Landweber (1942) with a model of infinitely long rows of point vortices, similar to the classical von Kármán analysis of a single vortex street. Stability conditions were obtained by noting that the mutually induced transverse velocities should be zero, and that the convection speed must be the same for all vortices. It was concluded from the former that the vortex streets must either be in-phase or in-antiphase, and, from the latter, that the circulation of the outer vortices must be larger for the in-antiphase mode (or smaller for the in-phase mode) than those of the inner vortices. Here, outer refers to vortices located towards the free stream and inner to vortices located towards the centreline (see figure 2). In contesting this reasoning, Bearman & Wadcock (1973) pointed out

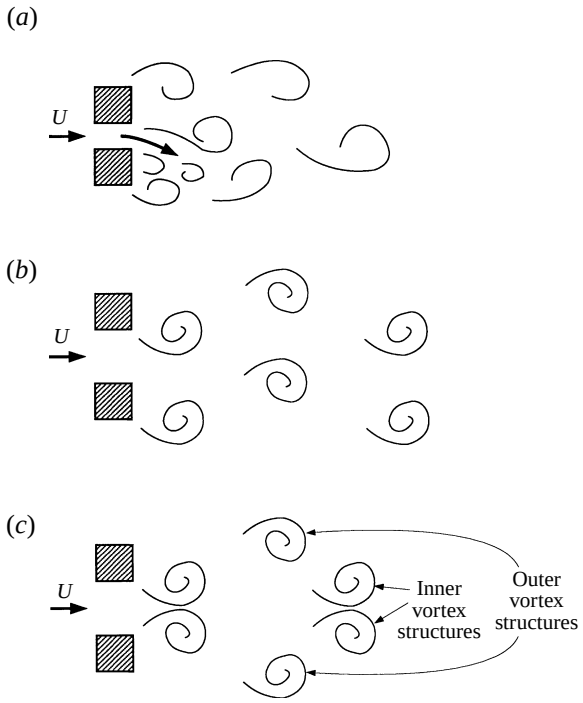

FIGURE 2. Sketch of three flow regimes as a function of gap/diameter ratio (g^*): (*a*) biased flow regime – $0.5 < g^* < 1$, (*b*) coupled vortex street regime, in-phase mode – $1 < g^* < 5$, (*c*) coupled vortex street regime, in-antiphase mode – $1 < g^* < 5$. Numerical values are based on observations of the circular-cylinder case, and so are only approximate for the square-cylinder case.

that pressure measurements on the cylinder surface indicated no pressure gradients in the separated flow region. Hence they argued that the symmetric pressure distribution implied equal circulation discharged into the wake region on either side of a given body.

Several numerical models of the two-cylinder flow have been published, including Stansby (1981) and Ng & Ko (1995) using discrete vortex methods for the high-*Re* case, and Chang & Song (1990) using a hybrid finite-difference finite-element model for the low-*Re* laminar-flow case. The basic qualitative features of the flow, such as the various flow regimes and modes, as well as the quantitative effects on drag and lift coefficients were successfully reproduced. Lack of velocity measurements, particularly unsteady or phase-averaged measurements, however precludes a more complete evaluation of the reliability and accuracy of the models. A numerical study of the present flow configuration by Bosch (1995) has been completed and will be reported elsewhere.

Recent measurements of ensemble-averaged turbulence statistics of the two-dimensional near-wake of single bluff bodies provide a rich basis for comparison with the present results. Much of the discussion has focused on flow topology, characterized by critical points, and its relation to turbulence statistics (Cantwell & Coles 1983; Zhou & Antonia 1994; LERP). There remains debate on the appropriate determination, conceptual as well as operational, of these points and their precise role, but their importance with regard to turbulence production is generally accepted. Centres, loosely characterized by closed streamlines, are associated with high vorticity and turbulent

kinetic energy (normal Reynolds stresses), while saddles, loosely characterized by converging and diverging streamlines, are associated with high Reynolds shear stresses and turbulence production. In an earlier laser-Doppler study of flow around a single square cylinder, LERP noted some deviations from this general picture, particularly in the base region, i.e. within the first four diameters behind the body. For example, turbulence production at centres could be comparable or even exceed that at saddles. Even in the near-wake region farther downstream, the highest Reynolds shear stresses occurred upstream of, and closer to the cylinder centreline than, saddle points.

Because the dominance of a single frequency is especially amenable to ensemble averaging, the present study deals primarily with the coupled regime. A study of this regime also allows a re-examination of the controversy regarding the inequality of the circulation of inner and outer vortex structures. Information regarding vortex motion and the relevant length and time scales is sought. The main interest lies in the relationship between the phase-averaged flow field and the turbulence statistics and the exchange of vorticity across the centreline and between adjacent structures through turbulent stresses. The characteristics of coupled vortex streets are compared in detail with those previously noted in one-cylinder streets. The differences between inner and outer structures and the extent to which either is similar to the one-cylinder structure are examined. The results shed light on critical points, their relation to invariant measures and turbulence characteristics, and hence give insight into not only two-cylinder flows but also one-cylinder and possibly free turbulent shear flows in general. Though recent work has highlighted the importance of three-dimensional aspects (Hayakawa & Hussain 1989; Zhou & Antonia 1994), measurements in the spanwise direction were not feasible, and so the discussion is restricted to two-dimensional aspects.

2.1. *Notation, non-dimensionalization and terminology*

Common notation and terminology are here summarized. The coordinate system in which the results will be presented is defined in figure 1. Unless otherwise specified, the cylinder diameter, D, and a reference velocity (to be defined below), U_0, is used throughout the following to non-dimensionalize all quantities, and Re and St are defined in terms of these parameters. The centreline refers to the line $y = 0$, while the cylinder centreline refers to the streamwise line through a cylinder centre (here, at $y = 1.5$). The region in the wake close to the cylinder ($x < 4$) is termed the 'base' region, while the region farther downstream ($x > 4$) is termed the near wake. LERP based the qualitative distinction between the two regions on whether the structure in that region has been completely shed (the near wake) or remains linked to the separating shear layer (the base region). The dividing value of $x = 4$ is somewhat arbitrary, but is convenient in a discussion of qualitative changes in the behaviour of flow characteristics. Inner and outer features (e.g. structures, shear layers) refer to features that develop towards the centreline (inner) and towards the free stream (outer) (again see figure 2). Centres and saddles are defined in terms of streamlines in a reference frame moving with vortex structures, and these are identified from a visual inspection of plotted streamlines.

According to the triple decomposition of a phase-varying signal, an instantaneous quantity, $f = \langle f \rangle + f' = \bar{f} + \tilde{f} + f'$, where $\langle f \rangle$ is the ensemble- or phase-average of f, $\bar{f}$ is the average over all phases, $\tilde{f}$ is the periodic component with zero mean, and f' is the 'incoherent' or 'turbulent' component. The time-average of f is denoted as $\bar{f}^t$. It is also convenient to use subscripts to denote a partial derivative with respect to the subscript, e.g. $f_x = \partial f / \partial x$.

	Reynolds number, Re		
g^*	15 000	22 000	30 000
1.0	Bistable, biased-gap flow	n/a	n/a
1.5	As for $g^* = 1$, but some switching to in-antiphase mode	n/a	n/a
2.0	Mostly stable in-antiphase mode	Mostly stable in-antiphase mode	In-antiphase mode with some switching to baised-gap flow
2.5	Mostly stable in-antiphase mode	Mostly stable in-antiphase mode	In-antiphase mode with short instabilities

TABLE 1. Qualitative observations of flow regimes for various g^* and Re

3. Experimental set-up, method and parameters

3.1. *Choice of experimental conditions*

The measurements were carried out in a closed water channel at the Institute for Hydromechanics, University of Karlsruhe, with a working cross-section measuring 56 cm $\times$ 39 cm. A pair of brass square cylinders, $D = 3$ cm, spanning the 39 cm with no endplates, was placed side-by-side, symmetric with respect to the channel centreline. This choice of cylinder size resulted in a blockage of 0.11, but allowed the installation of pressure transducers (piezo-electric, Kistler 701A) directly inside each cylinder (see figure 1).

Preliminary experiments using flow visualization were performed for a range of values of g^* and $Re = U_0 D/\nu$ (ν is the kinematic viscosity, and U_0 is the average approach velocity) to select a case for which more detailed laser-Doppler velocity measurements could be undertaken. Of particular interest were the regime and mode, since the stable in-antiphase mode was desired. The qualitative results are summarized in table 1. As expected, the biased-gap flow occurs for smaller g^*, but for $g^* \geqslant 2$, at moderate Re, the coupled in-antiphase mode was dominant. At the higher $Re =$ 30 000, short-term departures from the in-antiphase mode, either in the form of biased-gap flow at $g^* = 2$ or an approximate in-phase mode at $g^* = 2.5$, were more frequently seen. These limited results are consistent with those of Kim & Durbin (1988), who observed for circular cylinders that the mean time between a 'random' transition from one biased-gap flow to another tended to decrease with increasing Re. Whether a true Re-effect exists is unclear, since such effects are usually weak for sharp-edged bluff bodies. Based on these observations, the case chosen for the detailed measurements was $g^* = 2$, and $Re = 23\,100$, with $U_0 = 0.77$ m s^{-1}. As in LERP, the actual free-stream velocity downstream of the two cylinders was larger than U_0 because of blockage effects. These parameter choices placed the flow well within the coupled regime, with at the same time significant interaction between vortex streets in a stable in-antiphase mode, and could also be reasonably handled by the available signal processing equipment.

The time-averaged velocity profile measured at $x = -5$ is shown in figure 3, and displays, even at this upstream location, a difference between free-stream and centreline velocities of ≈ 0.04 (cf. for the one-cylinder case, LERP reported a corresponding value of ≈ 0.1 at $x = -3$). The turbulence level at this section was uniform and was $\approx 3.5\%$. LERP discussed possible effects of blockage and moderate free-stream turbulence levels at least on mean flow quantities. Since much of this work will compare

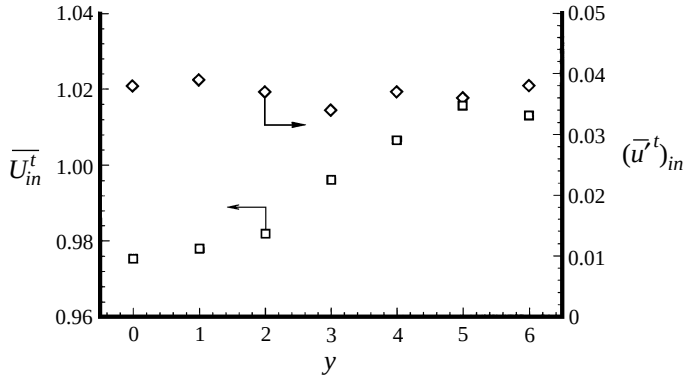

FIGURE 3. Time-averaged profiles at an inflow section, $x = -5$: □, velocity, $\overline{U_{in}^t}$; ◇, turbulence intensity, $(\overline{u'^t})_{in}$.

Parameter	Two-cylinder	One-cylinder
Re ($\times 10^3$)	23.1	21.4
Turbulence level (%)	≈ 3.5	≈ 2
Blockage (%)	11	7
Aspect ratio	9.75	9.75
Separation, g^*	2	n/a
Strouhal number, St	0.14	0.13
Measurement region	$1 \leqslant x \leqslant 9$	$-0.5 \leqslant x \leqslant 8$
	$0 \leqslant y \leqslant 4$	$0 \leqslant y^\dagger \leqslant 2.5$
Measurement mesh, Δx	0.33	$0.125^\dagger - 0.4$
Measurement mesh, Δy	0.33	$0.125^\ddagger - 0.25$

† For the one-cylinder case, $y = 0$ corresponds to the cylinder centreline.
‡ $(\Delta x, \Delta y) = (0.125, 0.125)$ only in $0 \leqslant x \leqslant 3$, $1.5 \leqslant y \leqslant 3$; outside of this region, Δx could be as high as 0.4, and $\Delta y = 0.25$.

TABLE 2. Experimental parameters for two-cylinder and one-cylinder (from LERP) cases

the single-cylinder results of LERP and the present results, and since the experimental conditions of both works were deliberately chosen to be comparable (see table 2), these effects were considered secondary within the scope of the present work. The average shedding frequency, f_s, was estimated from a pressure signal measured at a cylinder sidewall (see figure 1) to be $f_s = 3.6$ Hz ($\pm 10\%$). This yielded a Strouhal number, $St \equiv f_s D/U_0 = 0.14$, which is slightly higher than the value of 0.13 reported for a single square cylinder (e.g. LERP). Previous studies (Spivack 1946; Bearman & Wadcock 1973) concluded that St in the coupled regime is identical to that for a single body, though Landweber (1942) reported the contrary. In spite of the slightness of the difference, there may be grounds, to be elaborated on below, for believing that the difference may be significant.

3.2. *The LDV system and measurement region*

The same LDV system as in LERP was employed. It consisted of a forward-scatter two-channel system with Bragg cells for frequency shifting. The photomultiplier signals were filtered, amplified and digitized at 10 MHz (cf. maximum signal frequencies of 0.6 MHz) by a VUKO VKS 220-16 transient recorder. Doppler shift frequencies were

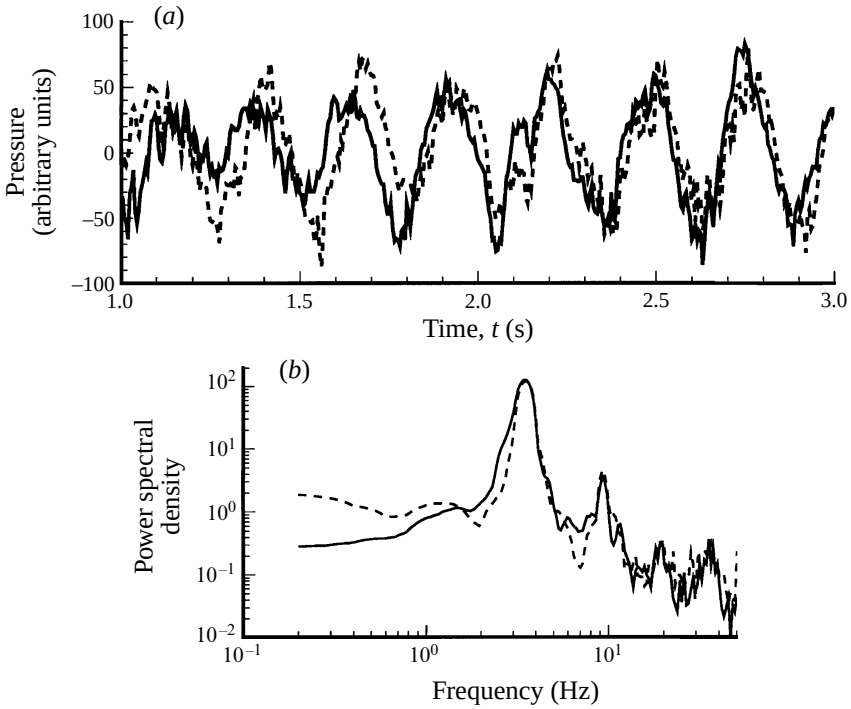

FIGURE 4. (*a*) Sample raw (unfiltered) pressure signals from each pressure transducer, (*b*) corresponding power spectra of pressure signals. Solid and dashed lines correspond to signals from different transducers.

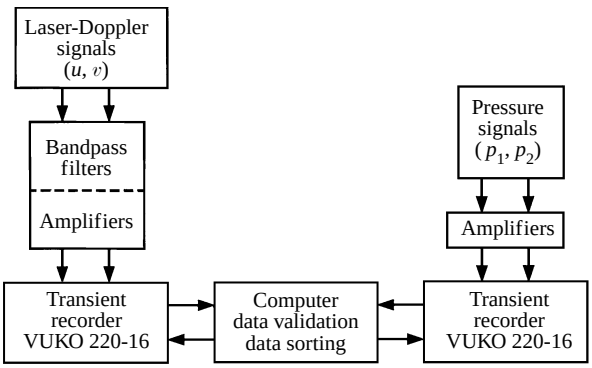

FIGURE 5. Schematic diagram of data acquisition system.

determined by software processing (emulating a counter) of digitized Doppler bursts. Primarily due to slowness in data transfer between transient recorder and computer, typical data rates were relatively low, varying usually in the range from 2 to 5 Hz. To reduce the measurement burden, it was assumed that, for the coupled in-antiphase mode, the ensemble-averaged flow was symmetric about the centreline, and hence measurements were taken only in the upper half of the flow ($1 \leqslant x \leqslant 9$, $0 \leqslant y \leqslant 4$). The measurement grid was regular with mesh size, $\Delta x = 1/3$ and $\Delta y = 1/3$; the grid in LERP was finer in the immediate vicinity of the cylinder (see table 2), but was comparable elsewhere.

3.3. *Phase definition*

To evaluate ensemble or phase averages, an appropriate phase or ensemble must be defined. The basic procedure used previously by Cantwell & Coles (1983) and LERP was followed here. A conditioning signal at a single fixed point in space (a pressure signal at the cylinder surface, see figure 1) provided a phase reference, implemented as a pressure peak. The 'events' between any two successive pressure peaks were assumed to constitute realizations of an ensemble, which is further subdivided into phase 'bins'. Events in each bin were taken to be statistically similar, so that meaningful averages could be computed. For the elucidation of the local structure of vortices, a phase reference at a fixed point in space becomes less relevant at distances far from that point (see the discussion of evolution jitter in Hussain & Hayakawa 1987, as well as in LERP). More local 'conditioning' schemes have been used when measurements have been made farther downstream (Hussain & Hayakawa 1987; Zhou & Antonia 1994), but the present study region is sufficiently small that the computed phase averages should still faithfully capture the structural features over most of the present measurement region is covered. Further, the aim of the present study is broader than previous studies of local vortex structure in that a more extensive region is covered. Because a structure may change significantly over this region, local conditioning is less appropriate.

In the case of two cylinders, as noted above, brief periods of in-phase shedding occur seemingly at random, even though the in-antiphase mode is dominant. The inclusion of these events in the averaging would violate the basic premise that the events in each ensemble should be statistically similar to each other. To identify these events so as to exclude them from the averaging, a pressure signal from the inner sidewall of each cylinder was taken. A segment of typical raw (i.e. unfiltered) signals from the two different pressure transducers and the corresponding (smoothed) spectra are shown in figure 4. Pressure signals during in-antiphase shedding were approximately in phase, though some lagging and leading are evident (e.g. for $1.5\ \text{s} < t < 1.8\ \text{s}$) for certain segments. A strong peak occurs in the spectra at the shedding frequency; a much smaller peak is also seen at a frequency of ≈ 9 Hz, but its significance is not clear since it is not a harmonic. The phase shift between the two pressure signals was used as an indicator of the in-antiphase shedding mode, with a zero phase shift reflecting the ideal case when vortex shedding occurs exactly in-antiphase. As in the one-cylinder case (Cantwell & Coles 1983), a dispersion in the frequency of each individual pressure signal was observed; more relevant to the present work, a dispersion in the phase shifts between the pressure signals was also found. The operational definition of an in-antiphase event in the present work was therefore based on a finite window size.

3.4. *Phase sorting*

A schematic diagram of the data acquisition system is shown in figure 5. A pressure transducer was installed within each cylinder, adjacent to a 1 mm diameter pressure tap. Both transducer signals were amplified before being digitized at 200 Hz by another VUKO two-channel transient recorder with a buffer size of 8 Kbytes per channel. When the buffers were full, the digitized signals were transferred to the computer, and a numerical low-pass filter with zero-phase-shift characteristic and cutoff at 5 Hz (cf. a shedding frequency of $f_s = 3.6$ Hz) was applied. The location of peaks in each signal was then found, and compared to each other to determine the phase shift between the two signals. A vortex shedding event was deemed to be in-antiphase if the phase shift was less than $\pi/4$. With this definition, more than 80%

of the events were accepted. Once the mode was verified, the actual phase assignment was performed with information from only a single transducer, that installed in the same half-plane where velocity data were measured. Thus, a single pressure time series was used for the actual phase sorting, with the other time series being used solely to identify the in-antiphase mode.

The synchronization of pressure and velocity data was achieved by starting the recording of pressure signals and validated LDV velocity realizations at a common time. Unlike LERP, in which synchronization was based on a transient recorder, the present work relied on the clock of the data acquisition computer. Due to the limited time resolution (10 ms) of the computer clock, only 8 phase bins were possible, corresponding to ≈ 4 clock ticks per bin. This phase resolution may be considered coarse in comparison to the 16 bins of Cantwell & Coles (1983) and the 20 bins of LERP, but it was considered consistent with the added uncertainties due to the phase shift between pressure signals. Additional validation criteria were also imposed, such that the shedding period was neither too short nor too long, and that the preceding and succeeding shedding cycle were acceptable. Each phase average was calculated from 400 samples resulting typically in 30–45 minutes of measuring time per point (i.e. the total number of accepted samples was 3200 at each measurement point), and the total number of measurement points was 325.

3.5. *Consistency of velocity data*

The mean as well as the phase-averaged flow is treated as a predominantly two-dimensional flow that is symmetric about $y = 0$. The consistency of the data with these basic model assumptions was checked in several ways. The flow rate estimated from integrating the velocity field in the cross-stream direction from $y = 0$ to $y = 4$ was constant to within $\pm$ 3% in the case of the mean field and within $\pm$ 5% in the case of the phase-averaged fields. Some of the discrepancy arises because $y = 4$ is not located in the undisturbed free stream, such that it does not constitute a real streamline (see the phase-averaged streamlines in figure 9), and hence there is some volume flux through the $y = 4$ measurement boundary. For the mean field, the local two-dimensional divergence $(\overline{u}^t)_x + (\overline{v}^t)_y > 0.2$ at only a single point, and for the phase-averaged field, at fewer than 8% of the measurement points. This value of 0.2 for the local divergence may be compared with typical maximum absolute values of mean and phase-averaged vorticities of 1.3 and 3 respectively.

Force measurements were not taken, but a rough estimate of $\bar{C}_D^t$ can be obtained from measured velocity profiles. Depending on the assumption regarding velocities towards the free stream outside the measurement region, $\bar{C}_D^t$ estimates ranged from 1.8 to 2.1. For a single two-dimensional square cylinder, a literature value of $\bar{C}_D^t \approx 2$–2.1 is typically found (LERP). For circular cylinders, $\bar{C}_D^t$-values for the two-cylinder case have been observed to be slightly higher (5%–10%) than those for the one-cylinder case (Bearman & Wadcock 1983). The uncertainty in the present $\bar{C}_D^t$ estimate is probably sufficiently large that slight differences cannot be distinguished.

In a flow symmetric about $y = 0$, both the mean and phase-averaged cross-stream velocity and the Reynolds shear stress should be zero. The average of $\overline{v}^t(x, y = 0)$ over all points on the centreline was 0.007 and individual absolute values were always less than 0.05. In the individual phases, the average of $\langle v \rangle(x, y = 0)$ continues to be small (< 0.02), but at individual locations, values up to 0.17 are attained and some systematic variations can be noticed. The average of $\overline{-u'v'}^t(x, y = 0)$ along the centreline was -0.009, with maximum absolute values of 0.022; the corresponding values for the phase-averaged quantity, $\langle -u'v' \rangle$, are similar with maximum absolute values reaching

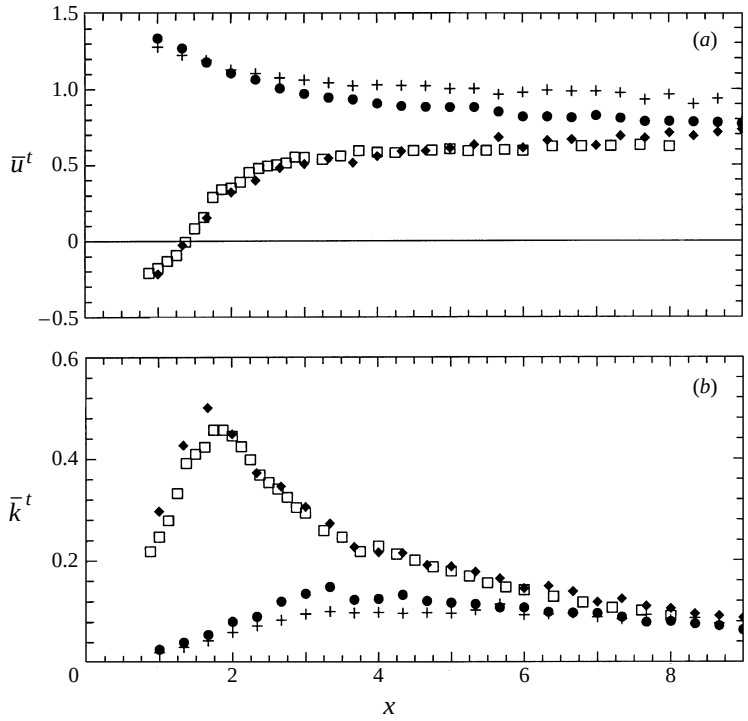

FIGURE 6. Streamwise variation of time-averaged characteristics: (*a*) velocities, $\overline{u}^t$, (*b*) turbulent kinetic energy, $\overline{k}^t$: ◆, two-cylinder case ($y = 1.67$); □, one-cylinder case ($y = 1.5$); ●, two-cylinder case ($y = 0$); +, two-cylinder case ($y = 3$). For the two-cylinder case, $Re = 23\,100$ and $g^* = 2$, while for the one-cylinder case, $Re = 21\,400$. In this and following figures, except where noted, the one-cylinder coordinates have been adjusted, so that cylinder centrelines are aligned.

0.05 only at isolated points. These values may be compared with typical maximum values of $\langle -u'v' \rangle$ and $\overline{-u'v'}^t$ of 0.15. While the evidence for symmetric mean fields is quite strong, the evidence for symmetric phase-averaged fields is more debatable. This should be kept in mind in considering the results to be presented in which symmetry of the phase-averaged fields about $y = 0$ has been implicitly or explicitly assumed.

4. Results

4.1. *The mean fields*

Since no information on the time-averaged fields is available in the literature, some results are discussed as a preliminary to the presentation of results on the phase-averaged fields. These are also relevant to the discussion of the argument of Bearman & Wadcock (1973) concerning the circulation discharged into the wake.

The streamwise variation of the mean velocity, $\overline{u}^t$, at three cross-stream locations (on the centreline, approximately on the cylinder centreline $y = 1.67$, and at $y = 3$) are shown in figure 6(*a*), together with the results for the one-cylinder case along the cylinder centreline. In the following, quantities on (or nearest to) the cylinder centreline are denoted with a *cc* subscript, while quantities on the centreline are denoted by an *c* subscript. The close agreement between $\overline{u}^t_{cc}$ for the one- and two-cylinder cases is notable. The mean recirculation region immediately behind the cylinder ends at

$x \approx 1.4$, which, within experimental scatter, is identical to the one-cylinder case (LERP). The sharp streamwise gradients in $\overline{u}^t_{cc}$ in the base region contrast with the slower evolution in the near-wake region. By the end of the measurement region, $\overline{u}^t_{cc}$ has recovered to ≈ 0.7, compared to ≈ 0.6 for the one-cylinder case. This difference is attributed primarily to increased mixing due to the higher turbulence levels prevailing near the centreline region compared to the free-stream turbulence levels in the one-cylinder case. Other secondary contributing factors include the slightly different transverse location ($y = 1.67$ is not exactly on the cylinder centreline) and increased levels of free-stream turbulence and particularly blockage. A jet-like flow in the gap region, with $\overline{u}^t_c$ attaining magnitudes of 1.4 (thereby exceeding even the velocities in the outer shear layer), develops into a wake-like flow by the end of the measurement domain, with $\overline{u}^t_c \approx \overline{u}^t_{cc}$. In marked contrast to the one-cylinder case, the flow is decidedly asymmetrical about the cylinder centreline as is clear from a comparison of the results at $y = 0$ and at $y = 3$. This already points towards asymmetries in the individual vortex streets and raises questions regarding their stability in the face of such asymmetry.

A similar picture is given by the streamwise variation of the mean (two-dimensional) turbulent kinetic energy, $\overline{k}^t \equiv (\overline{u'^2}^t + \overline{v'^2}^t)/2$ (figure 6*b*). A maximum of $\overline{k}^t_{cc} \approx 0.5$ is reached at about $x \approx 1.7$. A sharp growth and decline occur for $x < 4$ along the cylinder centreline, but for $x > 4$, the decay is very gradual. For $x > 2$ the $\overline{k}^t_{cc}$ for both one- and two-cylinder cases are practically indistinguishable, even towards the end of the measurement region. A small but consistent increase in $\overline{k}^t_{cc}$ for the two-cylinder case for $x < 2$ is noted, though its significance is not clear. The asymmetry of $\overline{k}^t$ about the cylinder centreline is rather weaker than was seen in $\overline{u}^t$, with $\overline{k}^t$ at $x = 9$ broadly uniform from $y = 0$ to $y = 3$. Only in the intermediate region, $2.5 < x < 5$, is the asymmetry about the centreline evident in $\overline{k}^t$.

Cross-stream profiles of various mean quantities at $x = 1$ and at $x = 8$ are compared in figure 7 with the corresponding results for a single cylinder, extended symmetrically across the cylinder centreline. The latter are plotted such that cylinder centrelines are aligned with each other. At $x = 1$, maximum velocities in the gap-jet flow are $\approx 5\%$ larger than those in the outer shear layer, and the wake is slightly wider, but the peak negative velocities, $\overline{u}^t \approx -0.2$, in the recirculation region are comparable to those for the one-cylinder case. LERP pointed out a double extremum in the $-\overline{u'v'}^t$-profile for the one-cylinder case; in the present results, only a single extremum is observed, but the measurement grid may have been too coarse to resolve a double extremum. Nevertheless, the quantitative similarity between the results for the one- and two-cylinder cases remains striking.

The approximate symmetry (or antisymmetry for $\overline{v}^t$ and $\overline{-u'v'}^t$) about the cylinder centreline ($y = 1.5$) would make it difficult to distinguish between the two cases on the basis of mean quantities. This is consistent with the finding of Bearman & Wadcock (1973) that the mean base pressure (for the two-circular-cylinder case) is essentially constant and does not exhibit any sign of asymmetry. For this value of g^*, the inner separated shear layers of the two cylinders do not appear to interact strongly. This accords with the one-cylinder results of Lyn & Rodi (1994), in which the phase-averaged separated shear layer at $x = 0.5$ was found to be confined to a region $y \leqslant 0.5$. By implication, the biased-flow regime, $g^* < 1$, may be viewed as beginning when the inner shear layers interact strongly. This does not necessarily imply that the effect of the other cylinder is negligible in all respects in the base region. Farther downstream at $x = 8$, as the wakes of the individual cylinders grow

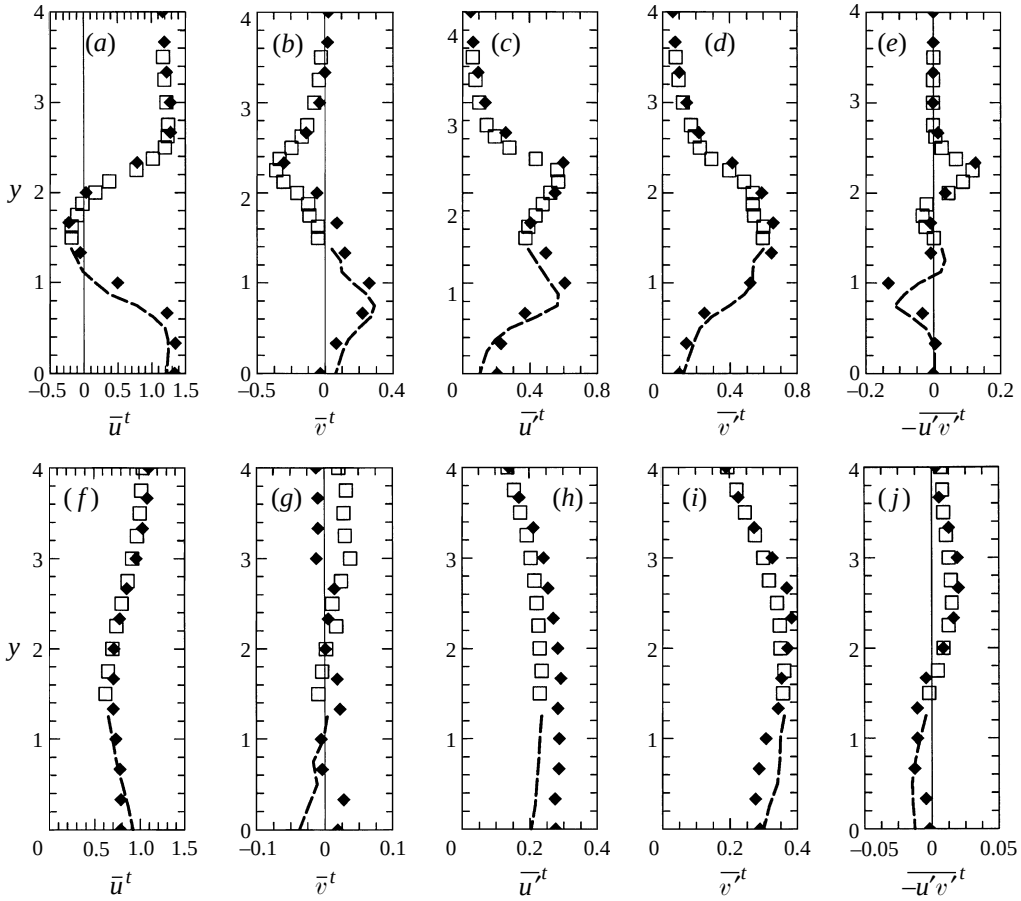

FIGURE 7. Time-averaged profiles of $\overline{u}^t$, $\overline{v}^t$, $\overline{u'}^t$, $\overline{v'}^t$, and $-\overline{u'v'}^t$ at $x = 1$ (*a, b, c, d, e*) and at $x = 8$ (*f, g, h, i, j*): ◆, two-cylinder case; □, one-cylinder case; – – – – –, symmetric extension of one-cylinder measurements.

laterally, the symmetry about the cylinder centreline deteriorates. This is evident in the profiles of $\overline{u}^t$, $\overline{u'}^t$, and $\overline{v'}^t$. The correspondence between one- and two-cylinder profiles remains however surprisingly good. Only in the $\overline{u'}^t$-profile, where $\overline{u'}^t$ in the two-cylinder case is larger than that in the one-cylinder case, is there a noticeable disparity.

4.2. *The phase-averaged velocity and streamfunction fields*

Examples of the phase-averaged velocity field (for typical phases 3 and 7) are shown in figure 8 in a frame of reference of a vortex structure in the near wake moving with a streamwise velocity of $U_c = 0.75$. The determination of this convective velocity is explained below. As will be the practice throughout, only the upper (measured) half of the flow is shown; the lower half is assumed symmetric about $y = 0$. The pattern of alternating circular flow, characteristic of a vortex street, is readily recognized. Figure 8 also indicates the measurement grid, as all measurement points are shown, and so can be compared to the scale of the vortex structures.

In figure 9, the streamlines are shown for phases 3 and 7 in a reference frame moving with a vortex structure; these were calculated by cross-stream integration of

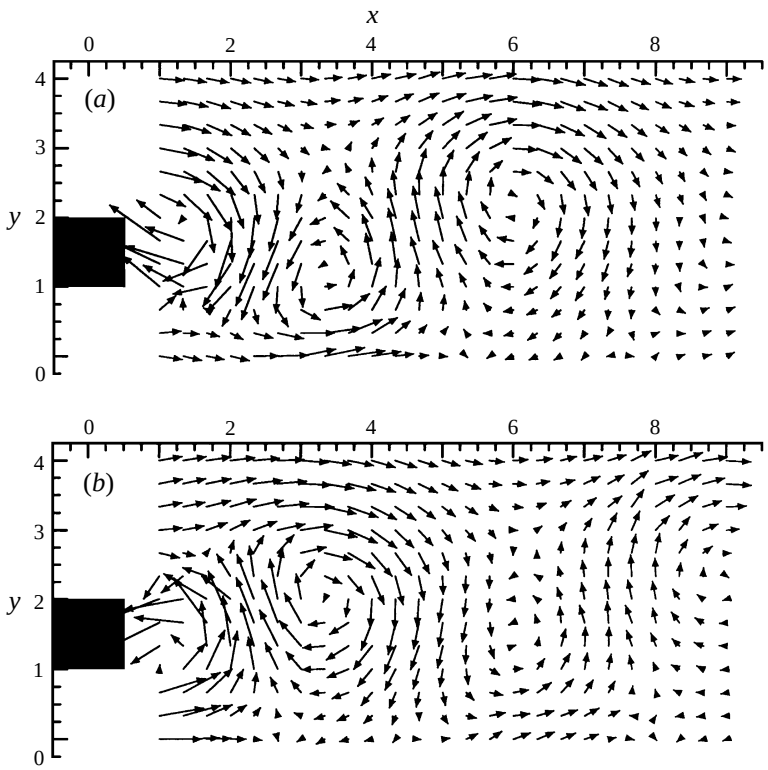

FIGURE 8. Velocity-vector plots from reference frame moving with a vortex structure for two-cylinder case at (*a*) phase 3 and (*b*) phase 7.

the translated $\langle u \rangle$-field from $y = 0$ to $y = 4$, assuming $y = 0$ to be a streamline. Vortex structures move at different speeds, but, as will be seen below, structures in the near wake move at approximately the same speed. For phase 3, an inner structure with centre at $(x, y) \approx (3.3, 1.2)$ is directly associated with an outer saddle at $(x, y) \approx (3.3, 2.8)$, in a configuration essentially the same as a one-cylinder single-centre-single-saddle system. The outer structure with centre at $(x, y) \approx (6.1, 2.2)$ is, however, associated with two, rather than one, saddles on the flow centreline, one at $x \approx 5.3$ and another at $x \approx 7.6$. For a flow symmetric about $y = 0$, converging and diverging streamlines at a saddle must be locally perpendicular to each other. Though a tendency in this regard is discernible, the inner saddles do not exactly satisfy this condition because of slight flow asymmetries, a relatively coarse measurement grid, and the limitations of the contouring software. The last-mentioned could be circumvented by reflecting the data about the flow centreline, but this was not done in order to make clear the uncertainties of the data. Since phases 3 and 7 are one half-cycle apart, the streamline pictures would be mirror images of each other if they had resulted from a one-cylinder flow. This is clearly not the case, as the inner saddles contrast with the outer saddles.

The anomalous streamline features around the centre at $x \approx 6$ in phase 7 merit comment. Circular motions in this region during this phase are weak (cf. the case in the same region at phase 3), and a more complicated flow topology may possibly result. Multiple regions of closed streamlines suggest multiple centres and saddles, akin perhaps to the flow pattern in a cavity flow. On the other hand, the weak-

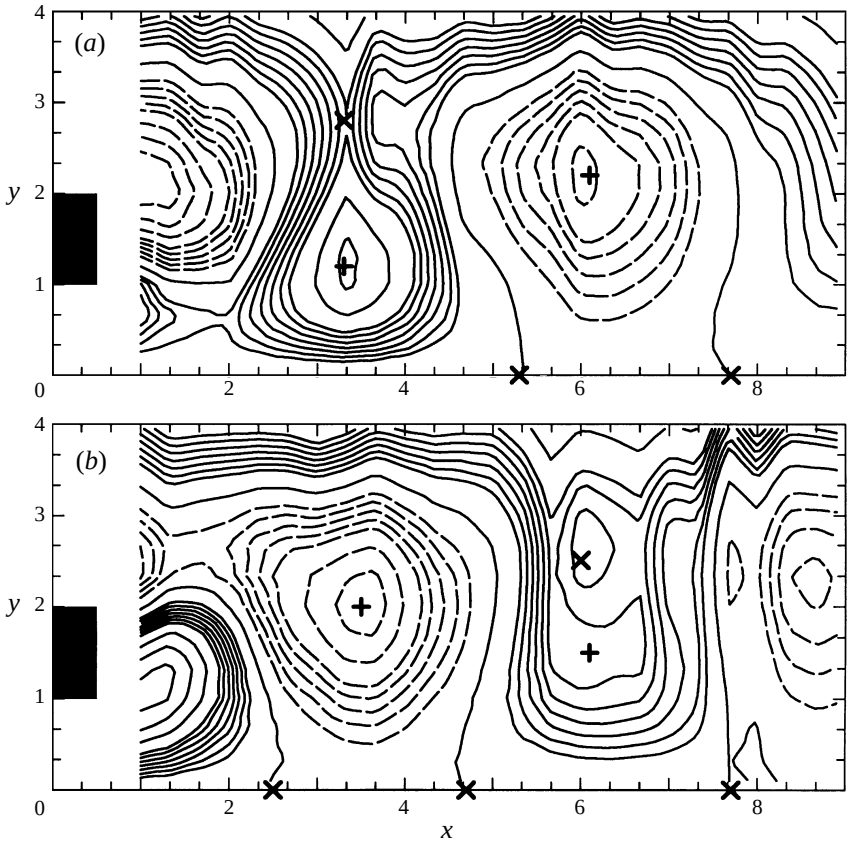

FIGURE 9. Streamline plots from reference frame moving with a vortex structure: (*a*) phase 3, (*b*) phase 7; contour values are not equidistant but were chosen to highlight centres and saddles. In this and following contour plots, the approximate locations of streamline centres (+) and saddles (×) are marked.

ness of the circular motions may make features more susceptible to noise or jitter. The centre identified in figure 9(*b*) at $x \approx 6$ may be considered the dominant or strongest centre, but the identification of a dominant saddle is more problematic. A rigid definition in terms of streamline convergence and divergence would place it to the left or even to the right of the position shown in figure 9(*b*). In the following, the labelled position of the saddle in this region at this phase should be considered quite cautiously, with more uncertainty in the streamwise direction than otherwise.

Though critical points in the near-cylinder region, $x < 2$, particularly saddles, are evident in figure 9(*b*), only those in $x > 2$ have been labelled because the present work focuses on structures which have been more or less entirely shed and are less influenced directly by the presence of the cylinder. Because of variations in the convection speeds of vortex structures, especially before they are shed, the locations of critical points in $x < 2$ are less reliably determined from the streamline plots. Many of the qualitative features of the fully shed structures to be discussed below are however also observed in the near-cylinder region.

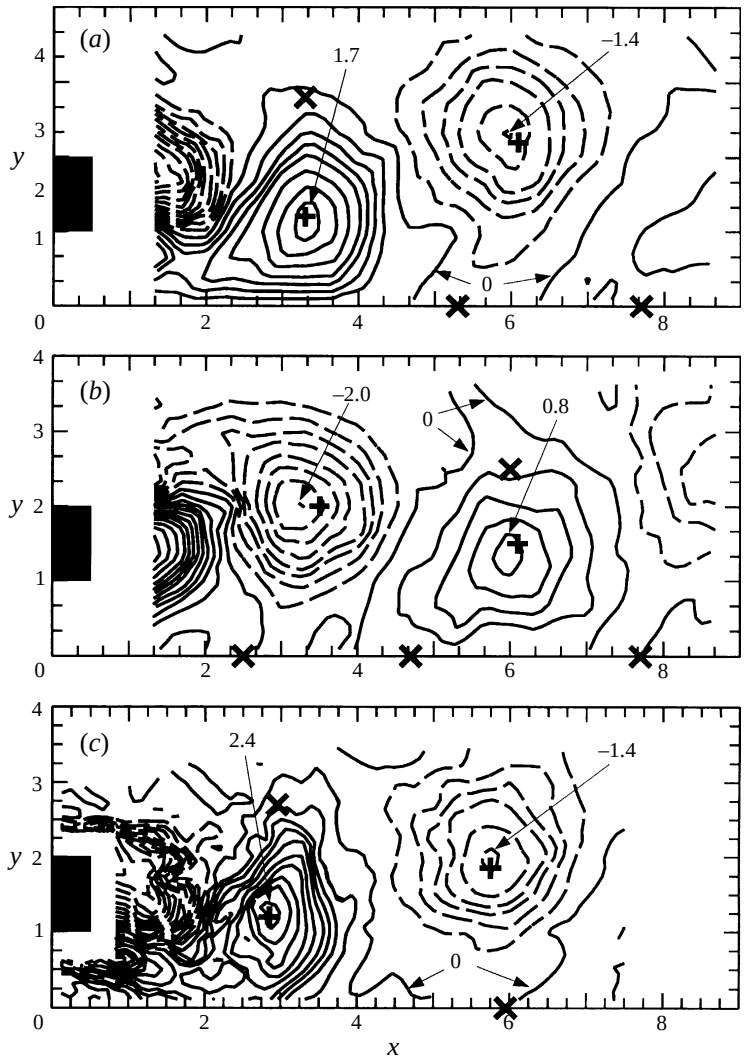

FIGURE 10. Contour plot of $\langle\omega\rangle$ for the two-cylinder case at (*a*) phase 3, and (*b*) phase 7, and (*c*) for the one-cylinder case at phase (9,19) (chosen to be most directly comparable to the two-cylinder phase 3 results): – – – – – , $\langle\omega\rangle < 0$; ——— , $\langle\omega\rangle \geqslant 0$; contour intervals, $|\langle\omega\rangle| \leqslant 0.8{:}0.2,\ 0.8 \leqslant |\langle\omega\rangle| \leqslant 2{:}0.3,\ 2 \leqslant |\langle\omega\rangle| \leqslant 3.6{:}0.4$.

4.3. *The phase-averaged vorticity and circulation*

Vortex structures become more apparent in the vorticity ($\langle\omega\rangle \equiv \langle v\rangle_x - \langle u\rangle_y$) contours of figure 10 for phases 3 and 7. In figure 10(*c*), $\langle\omega\rangle$-contours from the single-cylinder case are shown for the phase (phase (9,19) in LERP) most similar in terms of streamlines to phase 3 of the two-cylinder case. These phases will be used throughout this work for purposes of comparison. Gradients are computed using the same three-point centred scheme as in LERP. In addition, the (anti-)symmetry condition that the flow centreline is a line of zero vorticity has been imposed. Estimates of the locations of streamline centres and saddles for $x > 2$, based on streamline plots, have also been marked in figure 10 and the following figures. The vorticity distribution centred at $x \approx 6$ in phase 7 is seen to be quite regular and does not exhibit any

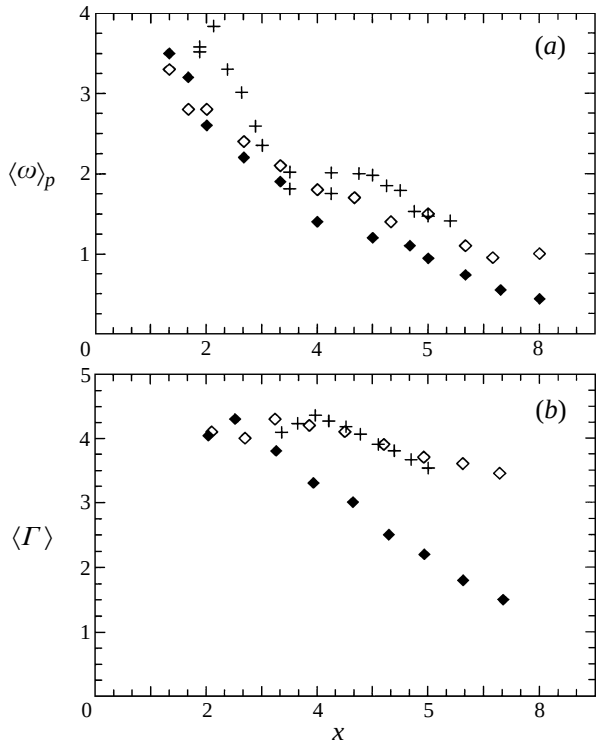

FIGURE 11. Streamwise variation of (*a*) peak vorticity, $\langle\omega\rangle_p$, and (*b*) circulation, $\langle\Gamma\rangle$: ◆, inner structure; ◇, outer structure; +, one-cylinder result.

unusual features that might have been expected from the corresponding streamline plot (figure 9*b*).

The presence of $\langle\omega\rangle$-extrema at $x \approx 6$, one positive and one negative, in each phase at the same streamwise location but on opposite sides of the cylinder centreline, indicates that the phase-averaging procedure has successfully captured the in-antiphase mode. It also shows that the convective speeds of outer and inner vortex structures are approximately the same throughout the measurement region, which is consistent with the approximate symmetry about the cylinder centreline, at least in the base region, of the mean velocity field. Since the mean field becomes more asymmetric about the cylinder centreline farther downstream, this raises the question of whether this equality of convective speeds can be maintained. The $\langle\omega\rangle$-distribution for the outer structure at $x \approx 6$ in the two-cylinder case resembles closely that of the one-cylinder case, even in the values of the peak $\langle\omega\rangle$, and suggests that the outer structure may be considered unaffected by the presence of the other cylinder. The constraining effect of symmetry about the centreline is however noted in a comparison of the two-cylinder inner structure in the base region with the corresponding one-cylinder structure, in which high $\langle\omega\rangle$-regions extend farther away from the cylinder centreline.

The comparative magnitudes of the vorticity extrema of the outer and inner vortex structures, denoted by $(\langle\omega\rangle_p)_o$ and $(\langle\omega\rangle_p)_i$ respectively, as well as for the one-cylinder case, as a function of x are shown in figure 11(*a*). In the base region, $(\langle\omega\rangle_p)_o \approx (\langle\omega\rangle_p)_i$ within experimental scatter, but both are smaller than the one-cylinder result. This comparison between one- and two-cylinder results in the base region should be cautiously interpreted since the measurement grid used by LERP is, in this region,

finer than the one used here, and may account for some of the difference. In the near-wake region, the decay of $\langle\omega\rangle$-peak values are reduced for both one- and two-cylinder cases. In view of experimental scatter, it does not appear that the values of $(\langle\omega\rangle_p)_o$ differ significantly from those of the one-cylinder case, but $(\langle\omega\rangle_p)_o$ is consistently larger than $(\langle\omega\rangle_p)_i$, reinforcing the view that the effects of the second cylinder are felt mainly by the inner structure.

The spatial distribution of the outer and inner structures in the near wake do not differ significantly either in extent or orientation, and so differences in vorticity peaks imply differences in the circulation, $\langle\Gamma\rangle$, associated with a vortex structure (figure 11*b*). As described in Cantwell & Coles (1983) and LERP, $\langle\Gamma\rangle$ was computed by a surface quadrature of $\langle\omega\rangle$. In the base region, $\langle\Gamma\rangle$ is approximately the same for both inner and outer structures, as would be expected from the values of the vorticity peaks. Because structures in the base region have not yet been fully shed, the estimate of $\langle\Gamma\rangle$ for a structure is not as straightforward as in the near wake, but since this applies to both inner and outer structures, the estimates should be reliable for comparative purposes. By contrast, in the near wake, a substantial difference is found, with $\langle\Gamma\rangle_o$ noticeably larger than $\langle\Gamma\rangle_i$. $\langle\Gamma\rangle_o$ agrees in value quite closely with $\langle\Gamma\rangle$ for the one-cylinder case in the near wake, as both decay slowly. The observation that the outer structure remains relatively unaffected while the inner structure is significantly affected indicates that the interaction between structures in the same vortex street is small compared to the interaction between inner structures of different streets.

The above results reconcile the theoretical prediction of Landweber (1942) with the experimentally based inference of Bearman & Wadcock (1973). The former had predicted that the circulation of the outer structure must be larger than that of the inner structure for the in-antiphase vortex street to be stable. Since the analysis assumes infinitely long rows of point vortices, its results are not applicable in the vicinity of a bluff body, but rather are justifiable only in the near wake where the coupled vortex streets are already fully established. The present results show that the outer-structure circulation beyond the base region is indeed larger than the inner-structure circulation, thus confirming the Landweber prediction. On the other hand, Bearman & Wadcock (1973) argued that unequal circulations were inconsistent with the symmetry of their measured time-averaged base-pressure profile. The present results show that, in the base region, not only is the time-averaged velocity field approximately symmetric about the cylinder centreline, but vorticity peaks and circulation for both inner and outer structures are comparable. This is consistent with the pressure measurements of Bearman & Wadcock. Thus, the conclusions of both Landweber and Bearman & Wadcock are correct, but they apply to different flow regions, and the two viewpoints are reconciled by a transition from a region of approximately equal circulation in the base region to a region of markedly unequal circulations in the near wake.

4.4. *Vortex structure motion*

The motion of vortex structures may be followed by considering the trajectory of a characteristic point in a vortex structure. This was chosen (following Cantwell & Coles 1983, and LERP) as the centroid of the vorticity distribution, because this could be more reliably estimated than e.g. the vorticity extremum. Figure 12(*a*) compares the trajectories of the inner and outer vortex structures as well as those associated with the one-cylinder case (with the cylinder centrelines aligned). Centroids of the outer vortex structures are located farther from the cylinder centreline than those of the one-cylinder flow, while those of the inner structures are quite close to the cylinder

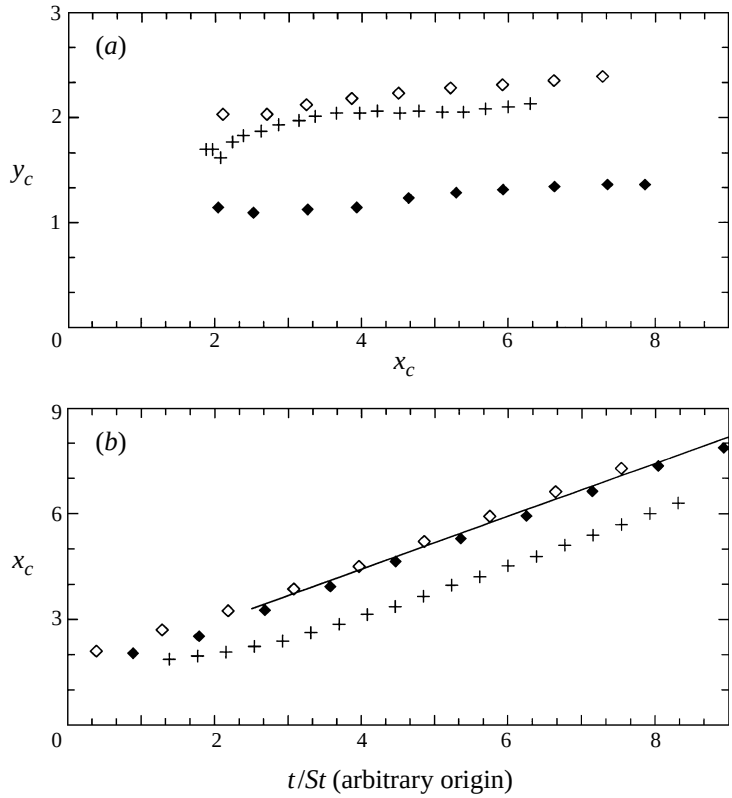

FIGURE 12. (*a*) Trajectory of centroids of inner and outer vortex structures, compared to that of a one-cylinder structure, (*b*) streamwise location of vortex structure centroids as a function of phase or time – the slope of the line is 0.75 and indicates an average vortex celerity in the near wake. Symbols as in figure 11.

centreline. The constraint of symmetry about the centreline confines the structures to the half-plane in which they are shed. As the structures develop and grow, they are forced to move away from the centreline, with the outer structure moving away, and the inner structure moving towards, the cylinder centreline.

In the base region, centroids of one-cylinder structures are found much deeper in the wake than centroids of outer two-cylinder structures. Because of the centreline constraint, the latter do not sweep as far across the wake as they would in the unconstrained one-cylinder flow. Thus, even in the base region, the centreline constraint is effective, as already noted in figure 11, possibly even leading to the slightly higher St observed. If the time that the outer structure spends in cross-stream motion is reduced, the frequency of shedding and hence St may be increased. This reasoning receives some support from the reduced streamwise separation, l_x, between successive structures of the same sign of vorticity in the near wake. This is found to be $l_x \approx 5.4$ compared to $l_x \approx 5.8$ for the one-cylinder case (LERP). The value of $l_x/2$ can be estimated from figure 12 by determining the difference in x_c at two phases one half-cycle apart (in figure 12*a*, every fifth point in the two-cylinder case). If vortices are shed more frequently, then, provided the convective speeds remain approximately the same, the distance between successive vortices will be smaller. The cross-stream separation, l_y, between

inner and outer structures in the near-wake region remains however comparable ($l_y \approx 1$) to that observed in the one-cylinder case, at least in the measurement region.

The streamwise location of the vortex structure centroids as a function of time (normalized such that the slope gives directly the streamwise convective speed) is shown in figure 12(*b*). In the near wake, both inner and outer structures move downstream with, within experimental scatter, the same velocity, $U_c \approx 0.75$. This is slightly smaller than that found for the single cylinder over the same region, where $U_c \approx 0.78$ (LERP). By $x = 8$, $\overline{u}^t(x, y = 0) = 0.79$, while $\overline{u}^t(x_c, y_c) = 0.75$, so that farther downstream, mean velocities in the neighbourhood of the inner structure will likely become smaller than the convective speed if the latter remains the same. At low-*Re*, the in-antiphase mode of coupled vortex streets, in contrast to the in-phase mode, was found to be stable in the sense of being maintained far downstream of the cylinders (Williamson 1985). With the growing asymmetry in the mean velocity profile and the circulation, it may be questioned whether this would also apply to the more turbulent case at higher *Re*. The Landweber stability argument assumed constant circulation, and so would not necessarily apply to the case where outer-structure circulation remained approximately constant but inner-structure circulation continue to decay sharply.

Comparison of the one- and the two-cylinder results for the vortex celerity also reveals a difference in the base region. In the one-cylinder case, a reduction in U_c (to ≈ 0.46) is evident, but in the two-cylinder case, this is much less obvious. This effect may be partially attributed to the enhanced jet flow in the gap, which is weaker in the one-cylinder case. At the present value of g^*, however, the jet flow, while measurable, is not strong. The effect may however be reinforced by the cross-stream constraint on vortex structure motion, so that streamwise motion is promoted at the same time that cross-stream motion is inhibited. Hence, U_c in the base region is much closer to U_c in the near wake. This is qualitatively consistent with the measurements of Kim & Durbin (1988), who observed $U_c \approx 0.8$ in the base region of a biased-gap flow with two circular cylinders (cf. $U_c \approx 0.83$ in the near wake of a circular cylinder estimated from the measurements of Cantwell & Coles 1983).

4.5. *The periodic component*

The periodic quantities, $\tilde{u}\tilde{u}$ and $\tilde{v}\tilde{v}$, provide a measure of the strength of large-scale 'periodic' motion (figure 13). In a vortex-structure frame of reference, their distributions in space take on characteristic shapes shared by both one- and two-cylinder cases. Values are generally small in magnitude near centres, with unequal peaks perpendicular to the cylinder centreline ($\tilde{u}\tilde{u}$), or upstream and downstream of the centre ($\tilde{v}\tilde{v}$). Some qualitative differences between one- and two-cylinder cases may however be noted. For the one-cylinder case, the weaker $\tilde{u}\tilde{u}$-peak is found near the saddle (figure 13*c*); though this remains true for the outer saddle in the two-cylinder case, the inner peaks do not coincide with inner saddles, which are instead characterized by relatively small values (figure 13*a*). Further, the inner $\tilde{u}\tilde{u}$-peaks, which are located close to the centreline between saddles, are always larger in magnitude than outer peaks; in the one-cylinder case, peaks were located on alternating sides of the cylinder. The contours of $\tilde{v}\tilde{v}$ (figure 13*b*) show small measured values along the centreline; in the one-cylinder case, substantially larger values are found at comparable distances from the cylinder centreline (figure 13*d*). This not only reflects the centreline constraint, but also supports the approximate symmetry in phase-averaged quantities (perfect symmetry would result in $\tilde{v}\tilde{v} = 0$).

The broader effects on large-scale motion due to the presence of the other cylinder

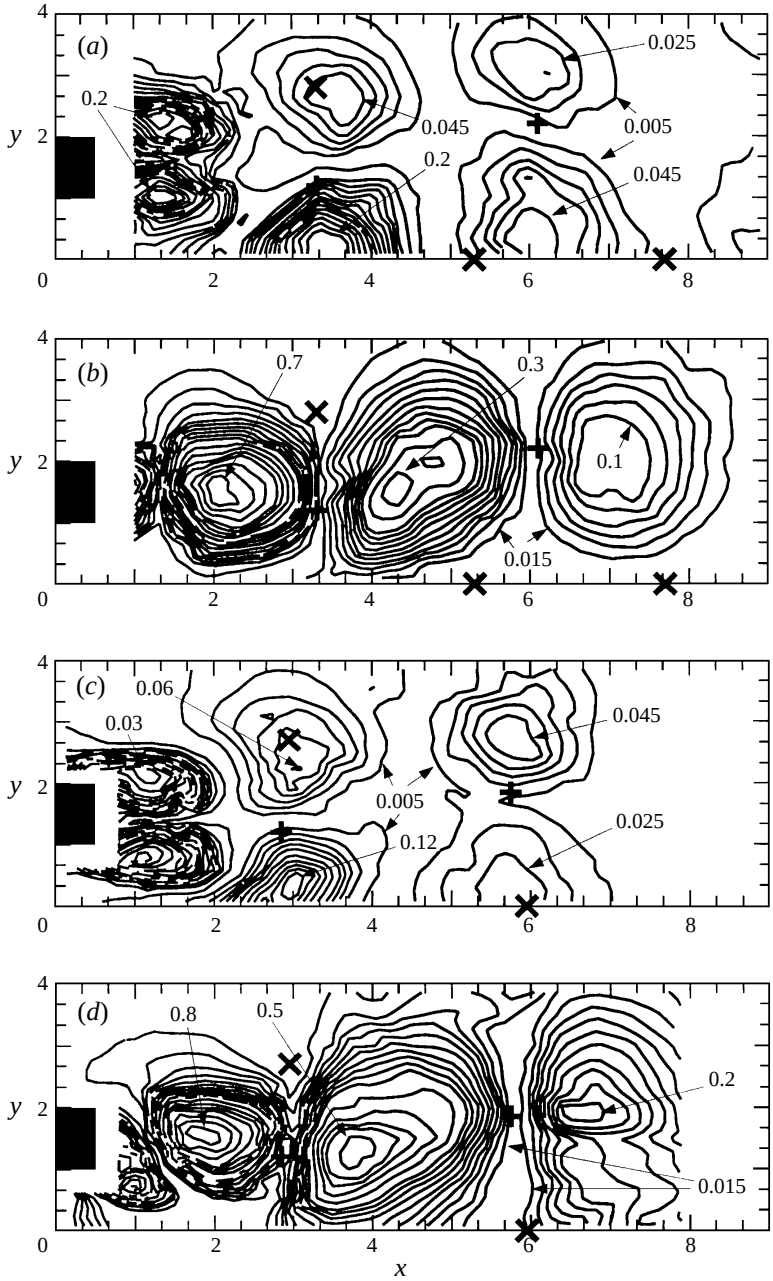

FIGURE 13. Contour plots of the periodic stresses for one- and two-cylinder cases: (*a*) two-cylinder $\tilde{u}\tilde{u}$ (phase 3), (*b*) two-cylinder $\tilde{v}\tilde{v}$ (phase 3), (*c*) one-cylinder $\tilde{u}\tilde{u}$ (phase (9,19)), (*d*) one-cylinder $\tilde{v}\tilde{v}$ (phase (9,19)). For $\tilde{u}\tilde{u}$-plots, contours intervals – $0.005 \leqslant \tilde{u}\tilde{u} \leqslant 0.045$: 0.01, $0.045 \leqslant \tilde{u}\tilde{u} \leqslant 0.12$: 0.015, $0.12 \leqslant \tilde{u}\tilde{u} \leqslant 0.2$: 0.02, $0.2 \leqslant \tilde{u}\tilde{u}$: 0.05; for $\tilde{v}\tilde{v}$-plots, contours intervals – $0.015 \leqslant \tilde{v}\tilde{v} \leqslant 0.06$: 0.015, $0.06 \leqslant \tilde{v}\tilde{v} \leqslant 0.1$: 0.02, $0.1 \leqslant \tilde{v}\tilde{v} \leqslant 0.2$: 0.025, $0.2 \leqslant \tilde{v}\tilde{v} \leqslant 0.4$: 0.05, $0.4 \leqslant \tilde{v}\tilde{v} \leqslant 1$: 0.1.

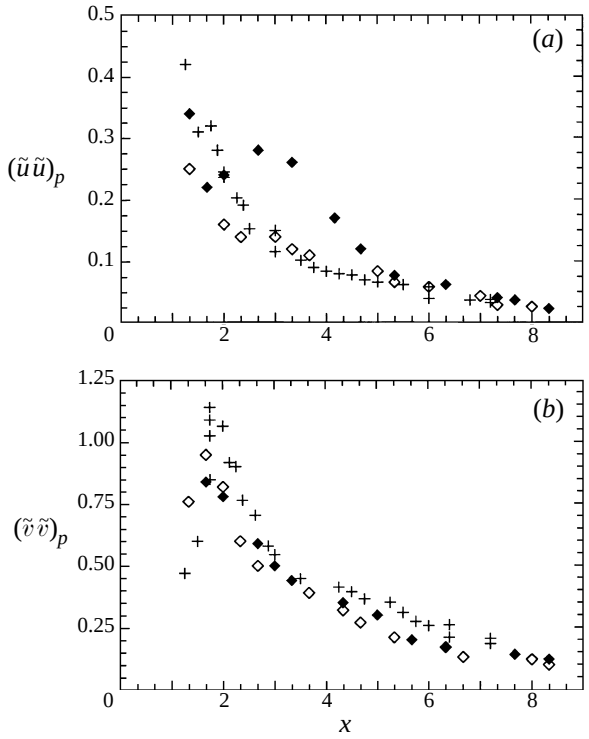

FIGURE 14. Streamwise variation of peak values of periodic stresses: (*a*) $(\tilde{u}\tilde{u})_p$, (*b*) $(\tilde{v}\tilde{v})_p$, (symbols as in figure 11). Inner and outer peak values are those associated with inner and outer structures.

are seen in the magnitudes of 'peak' values, $(\tilde{u}\tilde{u})_p$ and $(\tilde{v}\tilde{v})_p$, attained in one- and two-cylinder cases (figure 14). For the two-cylinder case, two peaks at a given section may be defined, corresponding to the passage of either an inner or an outer vortex structure, since, unlike the one-cylinder case, these are not necessarily comparable. Further, the passage of an outer structure may correspond, particularly for $(\tilde{u}\tilde{u})_p$, to a peak located near the centreline, hence an inner peak in the present terminology (see the outer structure in figure 13*c*). Towards the end of the base region (about $x \approx 3$–4), the $(\tilde{u}\tilde{u})_p$ of the inner structure is significantly larger than that of the outer structure, which in turn is approximately the same as the $\tilde{u}\tilde{u}_p$ of the one-cylinder case. In the near-wake region, differences between inner and outer structures (and one-cylinder structures) are surprisingly small. Differences between inner-structure and outer-structure values of $(\tilde{v}\tilde{v})_p$ are, in comparison, quite small throughout the measurement region. Both are nevertheless consistently smaller than single-cylinder results, particularly closer to the cylinder. These characteristics paint a picture of inhibition of cross-stream flow and enhancement of streamwise flow oscillations towards the centreline. Farther downstream, as the jet-gap flow develops into a more wake-like flow and the strength of the inner structure decreases, the differences from the single-cylinder results are much less pronounced.

4.6. *The turbulent component*

The distributions of two-dimensional turbulent kinetic energy, $\langle k \rangle$ ($\equiv [\langle u'^2 \rangle + \langle v'^2 \rangle]/2$) are shown in figure 15. These would be mirror images of each other about the cylinder centreline in a one-cylinder case, but the contours depart from the mirror-

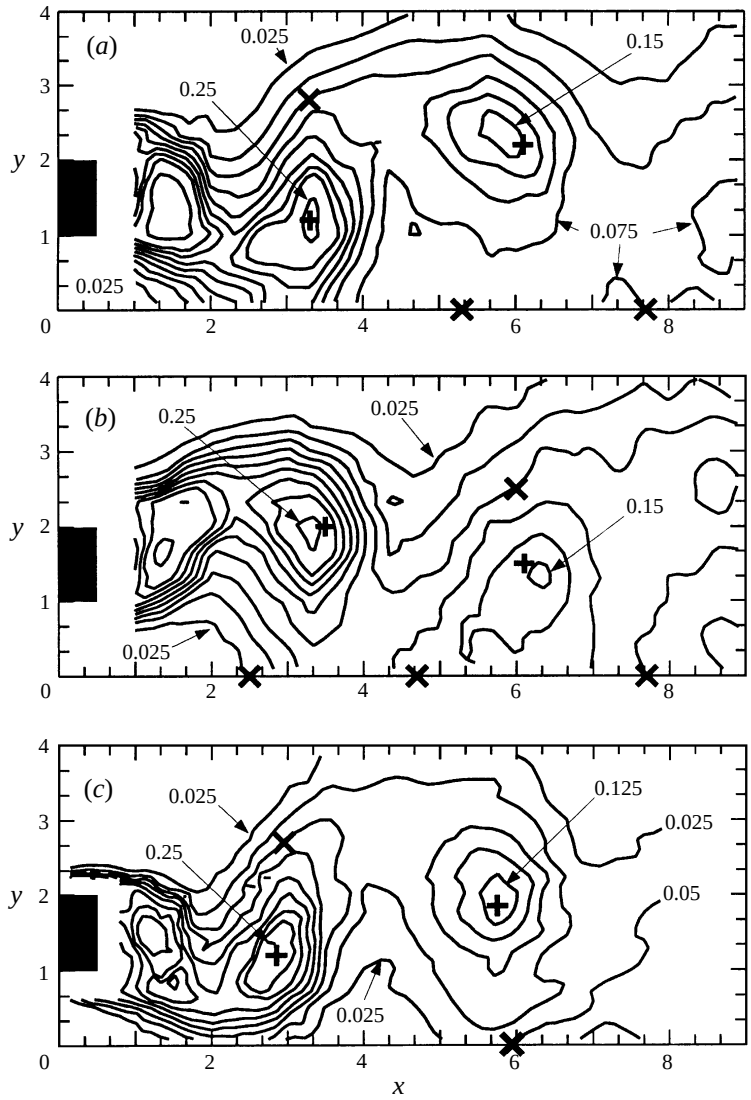

FIGURE 15. Contour plots of the turbulent kinetic energy, $\langle k \rangle$, for the two-cylinder case at (*a*) phase 3, at (*b*) phase 7, and (*c*) for the one-cylinder case at phase (9,19). Contour intervals $\langle k \rangle \leqslant 0.2 : 0.025,\ 0.2 \leqslant \langle k \rangle : 0.05$.

image scenario most clearly in the near wake, with more extensive regions where $\langle k \rangle > 0.1$ towards the centreline. Unlike the one-cylinder case with the free stream on both sides of the cylinder, the two-cylinder flow around each cylinder is bounded by a low-turbulence free stream on only one side, with the other side being a quasi-symmetry boundary with high turbulence levels. This is also clear in a more direct comparison of the one- and two-cylinder cases (figures 15*a*,*c*), in which the $\langle k \rangle$-contours of the former exhibit a much more sinuous form, with deep incursions of free stream flow into the wake. The two-cylinder wake near the cylinder (e.g. at $x = 1$) is wider (as defined by the $\langle k \rangle = 0.025$ contour) than the one-cylinder wake, which was already hinted at in the time-averaged results. The flapping separated shear layer does not approach the cylinder sidewall as closely as in the one-cylinder case, and

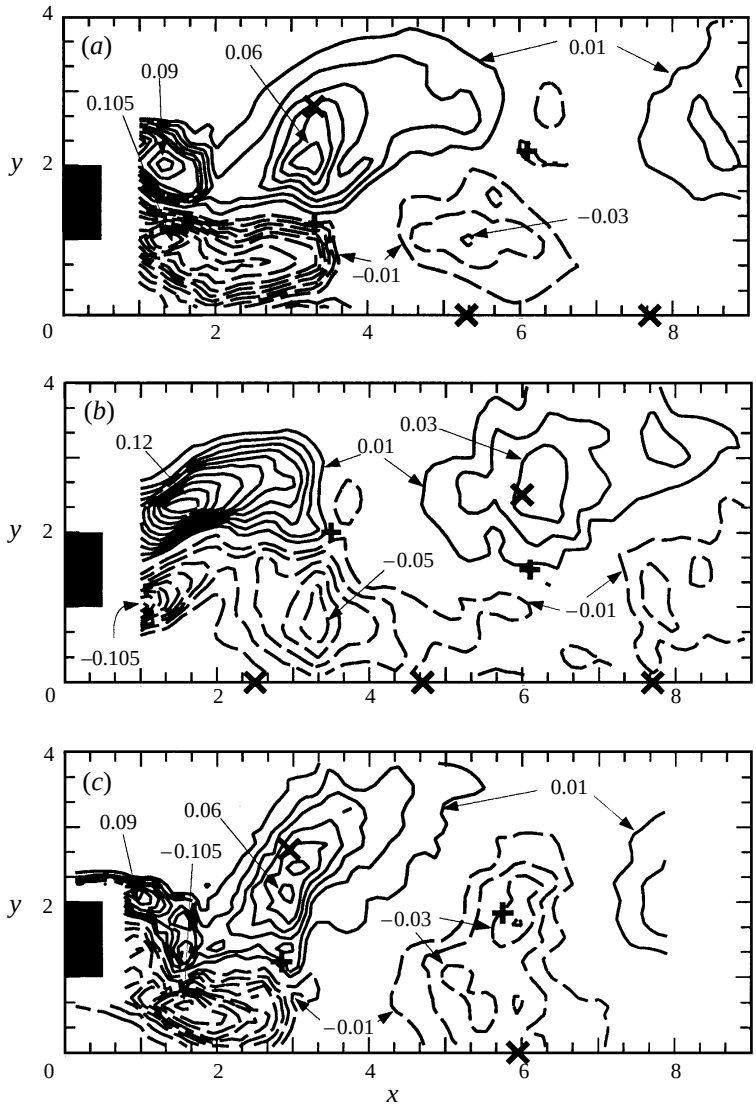

FIGURE 16. Contour plots of the Reynolds shear stress, $\langle -u'v' \rangle$, for the two-cylinder case at (*a*) phase 3, at (*b*) phase 7, and (*c*) for the one-cylinder case at phase (9,19). – – – – – , $\langle -u'v' \rangle < 0$; ——— , $\langle -u'v' \rangle \geqslant 0$; contour intervals, $0.01 \leqslant |\langle -u'v' \rangle| \leqslant 0.06 : 0.01$, $0.06 \leqslant |\langle -u'v' \rangle| : 0.15$.

hence the high-turbulence region remains in the free stream. Farther downstream, because of the less sinuous wake form, the two-cylinder wake may be the narrower in the sense of penetrating less into the free stream.

A somewhat similar picture is seen (figure 16) in the $\langle -u'v' \rangle$ contours. Measured values of $\langle -u'v' \rangle$ along $y = 0$ are used in figure 16, rather than imposing a symmetry condition, and so small measured values along the centreline emphasize that, even if perfect symmetry about the centreline was not achieved, this region is associated with negligible $\langle -u'v' \rangle$. The most notable difference between the two phases is the extensive region of high $\langle -u'v' \rangle$ around $x \approx 6$ at phase 7, compared to the rather restricted region at phase 3. At phase 7, a comparatively weak inner vortex structure

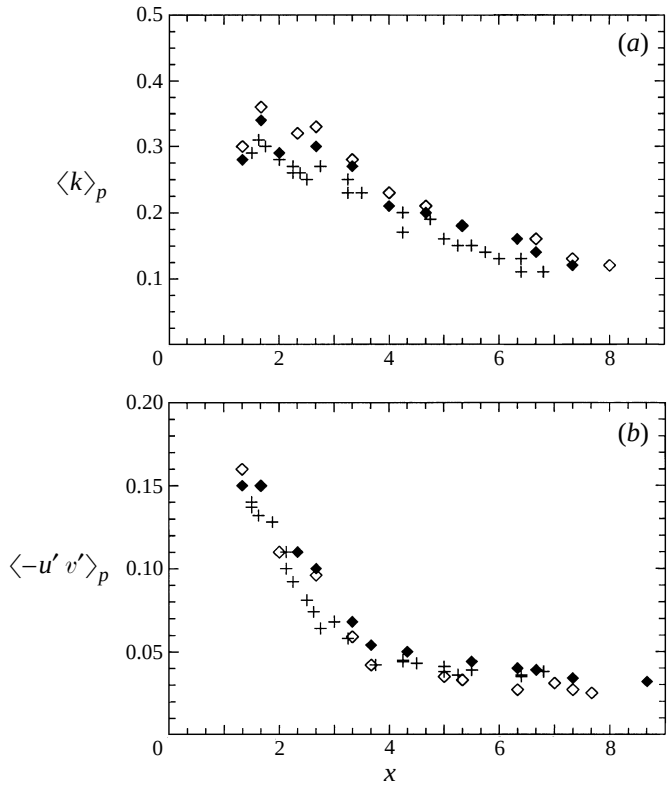

FIGURE 17. Streamwise variation of peak magnitudes of (*a*) $\langle k \rangle$, and (*b*) $\langle -u'v' \rangle$ (symbols as in figure 11). Inner and outer peak values are those associated with inner and outer structures.

passes through this region, though the extensive region of high $\langle -u'v' \rangle$ associated with it is found towards the free stream. The converse is true at phase 3 with a relatively strong outer vortex structure being associated with a much restricted region of high $\langle -u'v' \rangle$ towards the centreline. A comparison with the one-cylinder case (figure 16*c*) indicates that, in the absence of the other cylinder, a fairly extensive region of high $\langle -u'v' \rangle$ is observed in this region, more like the distribution seen at phase 7 in the two-cylinder case. LERP pointed out a 'leg' of high $\langle -u'v' \rangle$ extending through the vortex centre in the one-cylinder case; similar though much weaker features may be seen in the two-cylinder case at phase 3, but not at all at phase 7. This is attributed to the enhanced streamwise motion in the two-cylinder case. A strong link between the vortex structure and the $\langle -u'v' \rangle$-distribution moving in its immediate vicinity does not therefore seem to exist. Rather, the $\langle -u'v' \rangle$-distribution is apparently primarily determined by local flow conditions rather than by the characteristics of the vortex structure.

The streamwise variation of peak magnitudes of turbulent kinetic energy, $\langle k \rangle_p$, and Reynolds shear stress, $\langle -u'v' \rangle_p$, for one- and two-cylinder cases are compared in figure 17. For the latter, the quantities associated with inner and outer vortex structures are distinguished. Similar to $\tilde{u}\tilde{u}_p$ in figure 14, peaks in $\langle -u'v' \rangle_p$ at a given station during the passage of an outer (inner) structure are found in the inner (outer) region (figure 16). Differences between inner- and outer-structure peaks are slight but rather consistent, with outer structures generally being associated with larger $\langle k \rangle_p$

and smaller $\langle -u'v' \rangle_p$, as previously seen in figures 15 and 16 at specific phases. For outer structures, $\langle k \rangle_p$ occurs towards the free stream but $\langle -u'v' \rangle_p$ occurs towards the centreline. Thus, peaks, whether in $\langle k \rangle$ or $\langle -u'v' \rangle$, that occur towards the centreline tend to be lower than peaks that occur towards the free stream. $\langle k \rangle_p$, whether inner or outer, for the two-cylinder case is larger than for the one-cylinder case. This might have been expected since the centreline is a region of high turbulence levels rather than a low-turbulence free stream. For both one- and two-cylinder cases, $\langle -u'v' \rangle_p$ decays sharply in the base region, but then flattens noticeably. In the sharp-decay region, $\langle -u'v' \rangle_p$ for the two-cylinder case tends to be noticeably higher than for the one-cylinder case, which may be due to the effect of the gap-jet flow. In the flat region, the inner and outer $\langle -u'v' \rangle_p$ tend to bracket the one-cylinder value.

4.7. *Vorticity transport and vorticity flux density*

A major question raised by the present work concerns the transport of vorticity across the centreline. In the absence of such transport, the marked decay in the circulation of the inner structures would be difficult to explain. On the other hand, the small measured values of $\langle -u'v' \rangle$ (ideally zero in a flow symmetric about the flow centreline) indicates that net momentum transport across the centreline is negligible. A distinction between momentum and vorticity transport needs to be drawn, which raises the question of how these are related.

The general three-dimensional equations for the phase-averaged vorticity vector (see the Appendix) can be specialized to the case of a phase-averaged two-dimensional flow, and an equation for the only non-zero component can be written as

$$\frac{\mathrm{D}\langle\omega\rangle}{\mathrm{D}t} = \frac{\partial}{\partial x}\left\{\frac{\partial}{\partial y}\left[\frac{\langle u'^2\rangle - \langle v'^2\rangle}{2} + \frac{\langle w'^2\rangle}{2}\right] - \frac{\partial}{\partial x}\langle u'v'\rangle - \frac{\partial}{\partial z}\langle v'w'\rangle + \frac{1}{Re}\frac{\partial\langle\omega\rangle}{\partial x}\right\}$$
$$+\frac{\partial}{\partial y}\left\{\frac{\partial}{\partial x}\left[\frac{\langle u'^2\rangle - \langle v'^2\rangle}{2} - \frac{\langle w'^2\rangle}{2}\right] + \frac{\partial}{\partial y}\langle u'v'\rangle + \frac{\partial}{\partial z}\langle u'w'\rangle + \frac{1}{Re}\frac{\partial\langle\omega\rangle}{\partial y}\right\}. \quad (4.1)$$

The right-hand side of (4.1) has been written in divergence form, and so the bracketed terms can be interpreted as fluxes. Measurements of the fluctuating velocity component, w', are not available, but its net contribution to (4.1) cancels out. A definition of 'effective' turbulent flux densities of $\langle\omega\rangle$ in the x- and the y-directions may therefore be motivated as

$$J^x = \frac{\partial}{\partial y}\left[\frac{\langle v'^2\rangle - \langle u'^2\rangle}{2}\right] + \frac{\partial}{\partial x}\langle u'v'\rangle, \quad (4.2a)$$

$$J^y = \frac{\partial}{\partial x}\left[\frac{\langle v'^2\rangle - \langle u'^2\rangle}{2}\right] - \frac{\partial}{\partial y}\langle u'v'\rangle. \quad (4.2b)$$

Previous discussions of (4.1) or its equivalent have focused on the turbulence terms as representing vorticity generation (Tennekes & Lumley 1972) or as determining the 'geometry' of the $\langle\omega\rangle$-field (Hussain 1983), but the above flux interpretation is equally natural. The example of laminar Poiseuille flow between two parallel plates may be cited (Segel 1977; see also Lighthill 1963). The viscous diffusive flux of vorticity in the y-direction, $-\nu\,\mathrm{d}\omega/\mathrm{d}y = \mathrm{d}(\tau/\rho)/\mathrm{d}y$ ($\tau/\rho = \nu\,\mathrm{d}u/\mathrm{d}y$ is the kinematic shear stress). With $\langle -u'v' \rangle$ identified as the analogous turbulent shear stress, its derivative in the y-direction should contribute to the turbulent vorticity flux in the y-direction as it does in (4.2*b*). Similarly, although the pressure does not appear in the vorticity equation, pressure gradients are associated with vorticity fluxes. In the same Poiseuille

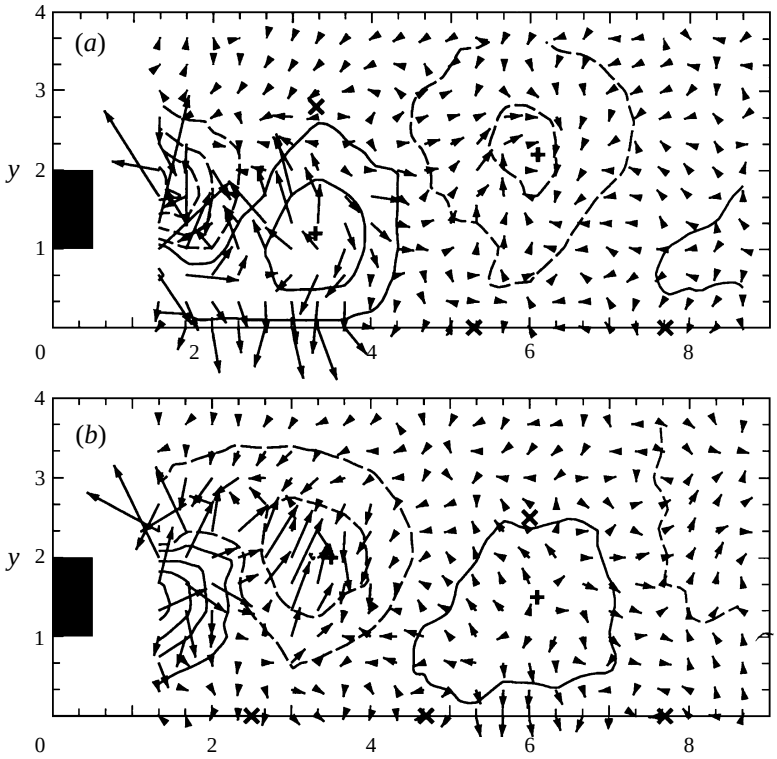

FIGURE 18. Vector plot of the turbulent vorticity flux density vector, $\boldsymbol{J}$: (*a*) phase 3, (*b*) phase 7. Vorticity contour values: $-3, -2, -1, -0.2$, 0.2,1,2,3.

flow example, the same vorticity flux is proportional to the pressure gradient in the streamwise direction, i.e. normal to the vorticity flux. If the terms involving the turbulent normal stresses are considered analogous to pressure, then gradients of these in the streamwise direction may contribute to fluxes in the cross-stream direction, again as in (4.2*b*).

The utility of defining the vector, $\boldsymbol{J} \equiv (J^x, J^y)$, lies in its relatively easy evaluation from measured quantities, and its visual presention in a vector plot (figure 18). Along $y = 0$, derivatives with respect to y were evaluated with a one-sided two-point finite-difference formula. $\boldsymbol{J}$ is generally directed from higher-$\langle\omega\rangle$ to lower-$\langle\omega\rangle$ regions, and relatively long vectors in the vicinity of the inner structures are directed across the flow centreline, illustrating the strength of the vorticity exchange between inner structures. In a flow that is strictly symmetric about $y = 0$, then $J^x(y = 0) = 0$, but, due to experimental scatter, this is not strictly observed. The two components of $\boldsymbol{J}$ for one phase are shown more quantitatively as contours in figure 19 together with estimated $\langle\omega\rangle = 0$ contours. J^x along $y = 0$ is negligible compared to its magnitude elsewhere. Though figures 18 and 19 are suggestive, it should be recalled that total turbulent fluxes would include gradients in $\langle w'^2\rangle$. Previous discussions (Tennekes & Lumley 1972; Hussain 1983) have neglected entirely terms involving the Reynolds normal stresses, but the present measurements indicate that these are not everywhere negligible compared to the terms involving the Reynolds shear stress.

The $\langle\omega\rangle = 0$ and $y = 0$ lines in figure 19 roughly delineate adjacent vortex structures, such that high-$\boldsymbol{J}$ contours crossing these contours are interpreted as indicating

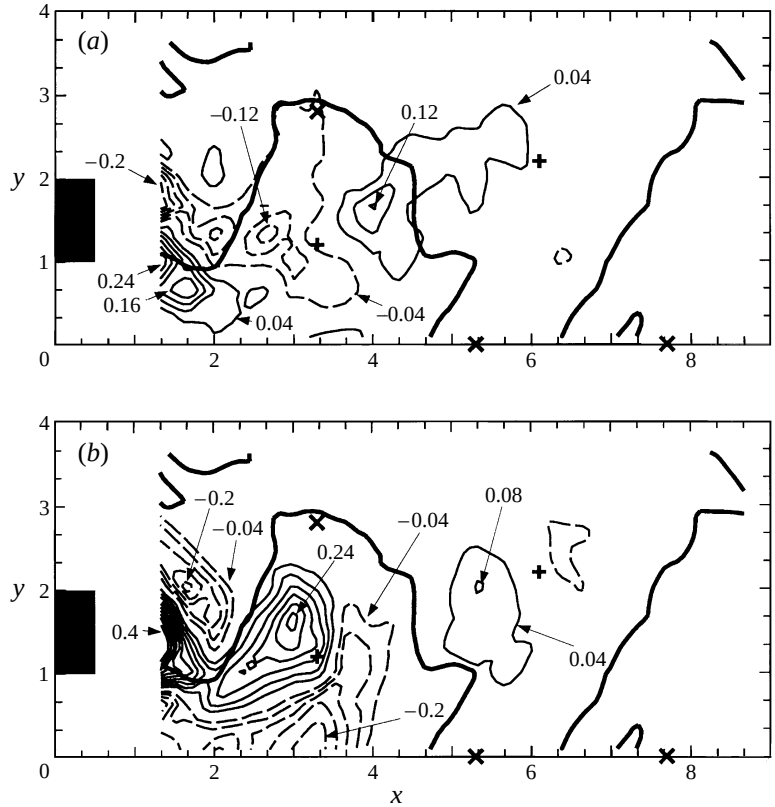

FIGURE 19. Contour plots of the separate components of $\boldsymbol{J}$ for phase 3: (*a*) J^x, (*b*) J^y, contour intervals – 0.4, except that the zero contour has been omitted. Thick solid lines indicate estimates of $\langle\omega\rangle = 0$ contours.

exchange between structures of differently signed vorticity. The most vigorous exchange occurs in the base region, primarily between vortex structures shed from the same cylinder, and secondarily between inner vortex structures shed from different cylinders. This is consistent with the dramatic decrease in circulation occurring in the base region, even in the one-cylinder case, as well as that occurring in the inner vortex structures. The significant exchange occurs not surprisingly towards the nose of the developing vortex structure, with high turbulent flux densities there in the downstream, upstream, and cross-stream directions. Inner and outer vortex structures in the base region differ most strikingly in the strong cross-stream flux densities on the centreline, compared to the corresponding weaker flux densities near the free stream. The outer structure in the near wake interacts primarily with the inner structure upstream of it, rather than with the downstream inner structure or the cross-stream outer structure. As noted previously, the inner structure interacts most strongly with the cross-stream inner structure, but upstream and downstream interactions also seem to be significant.

In addition to the $\langle -u'v'\rangle$-distribution already shown in figure 16, the distribution of $[\langle v'^2\rangle - \langle u'^2\rangle]/2$ (figure 20) is seen in (4.2*a*) and (4.2*b*) to be important for turbulent vorticity exchange and, as will be discussed below, also for turbulence production. A sinuous vortex street 'core' is found in which $\langle v'^2\rangle - \langle u'^2\rangle > 0$, with peak magnitudes decreasing sharply from the base region to the near-wake region. In the latter region, a local peak in $[\langle v'^2\rangle - \langle u'^2\rangle]/2$ is also often observed along the centreline. Between

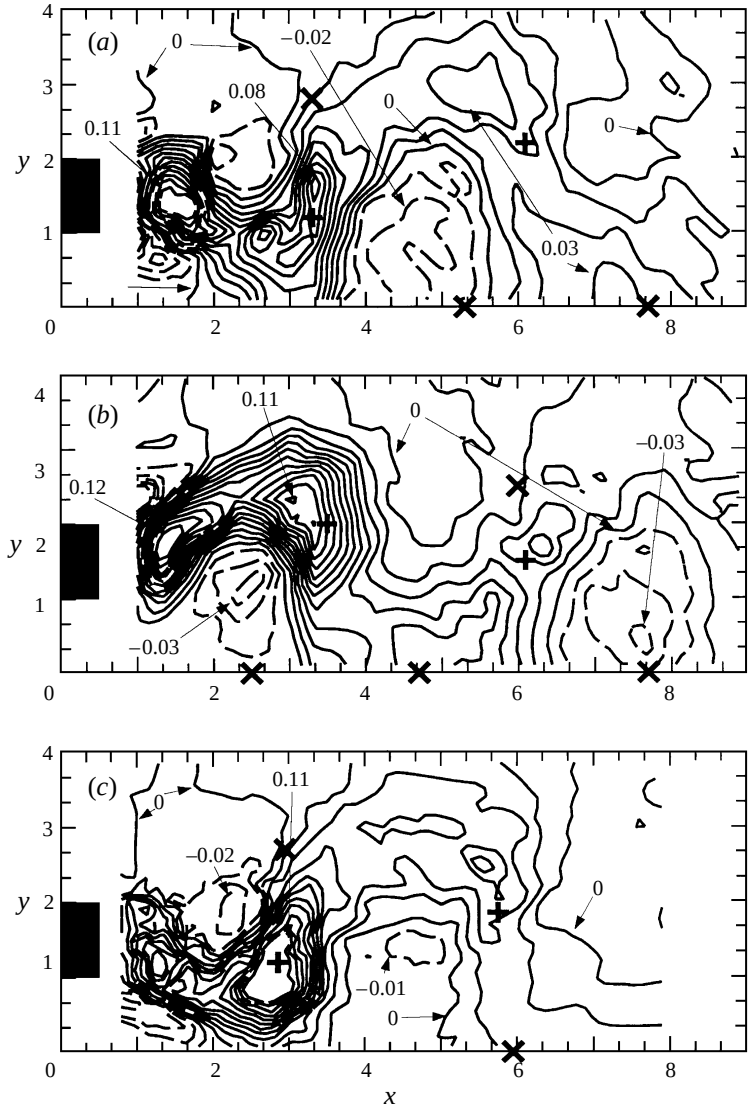

FIGURE 20. Contour plots of the quantity, $[\langle v'^2\rangle - \langle u'^2\rangle]/2$ for the two-cylinder case, (*a*) phase 3, (*b*) phase 7, and (*c*) for the one-cylinder case, phase (9,19); contour intervals $[\langle v'^2\rangle - \langle u'^2\rangle]/2 < 0.1 : 0.01$, $[\langle v'^2\rangle - \langle u'^2\rangle]/2 > 0.1 : 0.02$.

the folds of positive $[\langle v'^2\rangle - \langle u'^2\rangle]$ are substantial regions near the centreline where $[\langle v'^2\rangle - \langle u'^2\rangle] < 0$. The main difference between one- and two-cylinder cases, as well as inner and outer regions, lies in the extent of regions of significant negative $[\langle v'^2\rangle - \langle u'^2\rangle]$. The resulting sharper gradients in the region of the centreline enhance turbulent vorticity fluxes across $y = 0$.

4.8. *Turbulence production*

The two-dimensional turbulence production,

$$\langle P\rangle = -\langle u'^2\rangle\langle u\rangle_x - \langle v'^2\rangle\langle v\rangle_y + \langle -u'v'\rangle[\langle u\rangle_y + \langle v\rangle_x], \tag{4.3a}$$

$$= [\langle v'^2\rangle - \langle u'^2\rangle]\,\langle u\rangle_x + \langle -u'v'\rangle\,[\langle u\rangle_y + \langle v\rangle_x], \tag{4.3b}$$

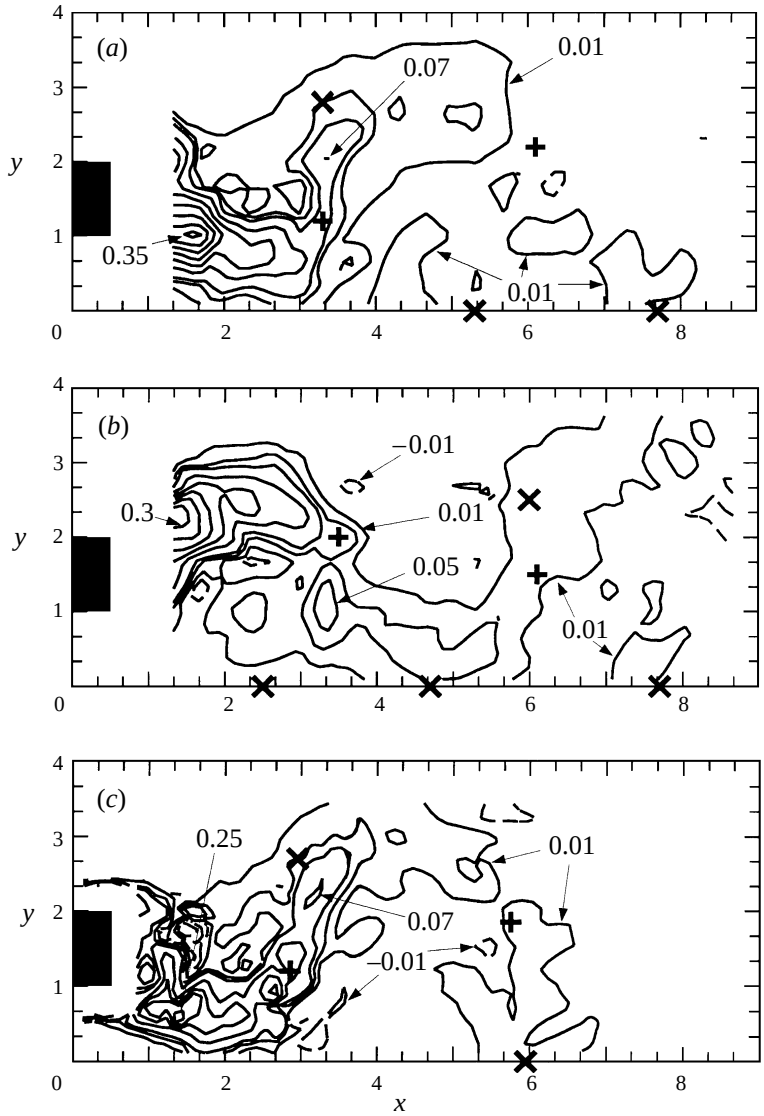

FIGURE 21. Contour plots of turbulence production, $\langle P \rangle$, for the two-cylinder case at (*a*) phase 3, at (*b*) phase 7, and (*c*) for the one-cylinder case at phase (9,19). – – – – –, $\langle P \rangle < 0$; ———, $\langle P \rangle \geqslant 0$; contour intervals $-0.01 \leqslant \langle P \rangle \leqslant 0.05$: 0.02, $0.05 < \langle P \rangle$: 0.05.

is a contraction of the Reynolds stress tensor, $\langle -u_i' u_j' \rangle$, with the velocity gradient tensor, $\langle \nabla \boldsymbol{u} \rangle$. Equation (4.3*b*) follows from plane continuity. As a scalar, $\langle P \rangle$ is invariant and, for a flow symmetric about the flow centreline, should also be symmetric about the centreline. As seen previously in figure 16, $\langle -u'v' \rangle$ is negligible along $y = 0$ because of flow symmetry, so $\langle P \rangle$ along $y = 0$ was evaluated in the following as $\langle P \rangle = [\langle v'^2 \rangle - \langle u'^2 \rangle] \langle u \rangle_x$. An overall qualitative similarity is found for the two-cylinder case at the two phases and for the one-cylinder case (figure 21), but several differences in detail are noted. The high-$\langle P \rangle$ region along $y = 0$, towards the downstream edge of inner structures (e.g. at $x \approx 4.3$ in phase 3 and at $x \approx 7.3$ in phase 7) does not have a counterpart in the one-cylinder case, which shows rather a slightly negative

production at $(x, y) \approx (3.1, 0.3)$. A comparable high-$\langle P \rangle$ region towards the free stream is also not evident for the outer structure; rather a negative-$\langle P \rangle$ patch similar to that seen in the one-cylinder case is observed at $(x, y) \approx (3.7, 2.7)$. The high-$\langle P \rangle$ region is due to more negative levels of both $[\langle v'^2 \rangle - \langle u'^2 \rangle]$ (as was previously seen in figure 20) and $\langle u \rangle_x$ as will be discussed below. The other high-$\langle P \rangle$ regions along $y = 0$ for the two-cylinder case are due to local highs in $[\langle v'^2 \rangle - \langle u'^2 \rangle]$ and positive $\langle u \rangle_x$, while, in the one-cylinder case, the non-zero $\langle -u'v' \rangle$ contribution becomes important.

A higher $\langle P \rangle$ is observed in the centreline region at $x \approx 5$ in phase 7 than in the corresponding outer region in phase 3 (recall that these phases would be mirror images in the one-cylinder case). On the other hand, a strip of significant $\langle P \rangle$ extends well into the outer near-wake region in phase 7, while the situation in phase 3 towards the centreline is noticeably patchy. This is also seen to a lesser degree in the one-cylinder results. Higher levels of $\langle P \rangle$ seem to be reduced more quickly in the inner region than in the outer region, which is likely related to the faster streamwise decay of $\langle -u'v' \rangle$ in the inner region. The high-$\langle P \rangle$ regions in the centreline region might be thought to contribute to the higher levels of $\langle k \rangle$ there in the two-cylinder case, but the implications of the more rapid reduction in $\langle P \rangle$ are less clear.

4.9. *A local velocity-gradient invariant*

Because of its direct relationship to the strain-rate and vorticity fields, the geometry of the phase-averaged flow field has been considered a key to an understanding of turbulence characteristics. A number of approaches have been proposed, but they share however a basis in $\langle \boldsymbol{\nabla u} \rangle$ (Chong, Perry, & Cantwell 1990; Wray & Hunt 1990; Zhou & Antonia 1994; Jeong & Hussain 1995). For general three-dimensional flows, these may lead to different predictions (Jeong & Hussain 1995), but for the predominantly plane flows considered in the present work, these all involve the (negative of the) second invariant of $\langle \boldsymbol{\nabla u} \rangle$,

$$\langle q \rangle = \langle u \rangle_y \langle v \rangle_x - \langle u \rangle_x \langle v \rangle_y, \tag{4.4a}$$

$$= \langle u \rangle_y \langle v \rangle_x + [\langle u \rangle_x]^2, \tag{4.4b}$$

where (4.4*b*) follows from (4.4*a*) by plane continuity. $\langle q \rangle$ is evaluated with a finite-difference approximation to (4.4*a*). Along $y = 0$, (4.4*b*) is used with the symmetry condition, $\langle u \rangle_y = 0$, and so $\langle q \rangle = [\langle u \rangle_x]^2$. In general, $\langle q \rangle$ may be directly related to the strain rate and vorticity by

$$\langle q \rangle = \langle s \rangle^2 - \tfrac{1}{4} \langle \omega \rangle^2, \tag{4.5}$$

where $\langle s \rangle = \{[(\langle u \rangle_y + \langle v \rangle_x)/2]^2 - \langle u \rangle_x \langle v \rangle_y\}^{1/2}$ is the two-dimensional principal rate of strain (Weiss 1991; Basdevant & Philipovitch 1994; Jeong & Hussain 1995). High $\langle q \rangle > 0$ or low $\langle q \rangle < 0$ at a point indicates respectively a dominance of strain rate relative to vorticity or vice versa.

As might be expected from (4.5), $\langle q \rangle$-minima (figure 22) are located close to $\langle \omega \rangle$-peaks. Regions of negative $\langle q \rangle$ tend however to be more restricted in extent than the corresponding $\langle \omega \rangle$-regions in both one-and two-cylinder cases, implying that strain begins to be important towards the edges of a vortex structure. Asymmetries in the vortex strengths between phases 3 and 7 are reflected in asymmetries in the minima of $\langle q \rangle$. The one- and two-cylinder results again share similar qualitative features. Each vortex structure may be associated with two relatively high-$\langle s \rangle$ regions, the more significant one being just downstream of the vortex centre, e.g. for the two-cylinder case in phase 3 at $(x, y) \approx (4.1, 0))$ or in phase 7 at $(x, y) \approx (4.6, 2.5)$, and the less

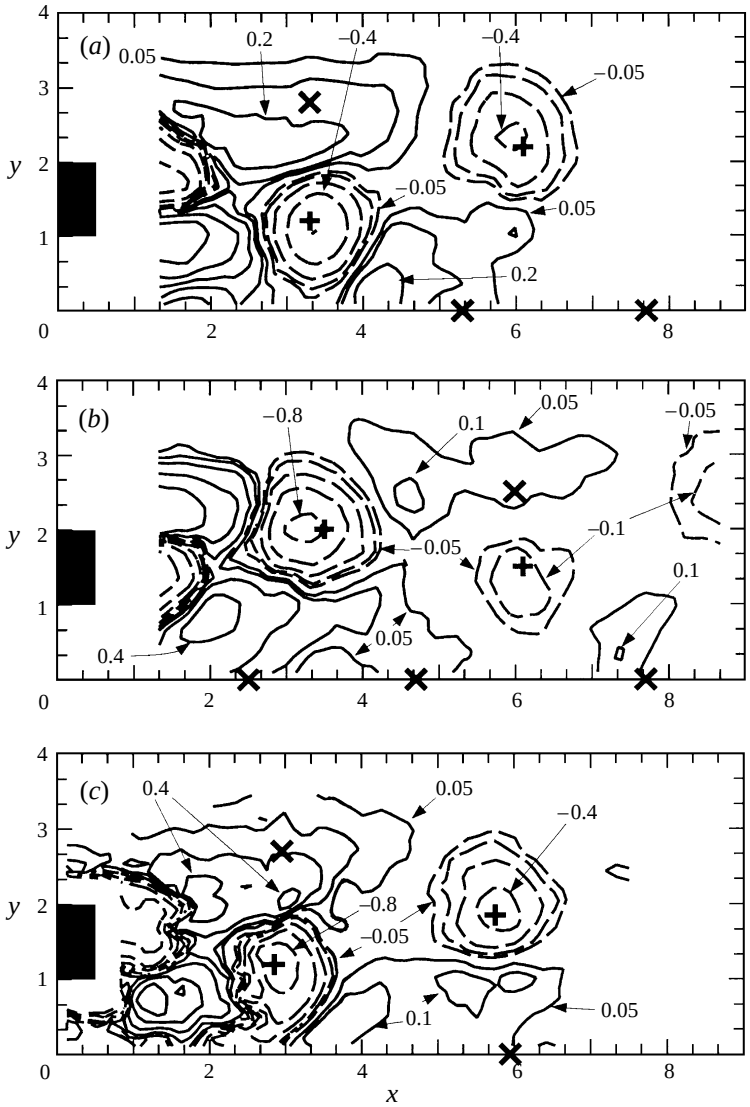

FIGURE 22. Contour plots of the invariant quantity, $\langle q \rangle$, for the two-cylinder case at (*a*) phase 3, at (*b*) phase 7, and (*c*) for the one-cylinder case at phase (9,19). – – – – – , $\langle q \rangle < 0$; ——— , $\langle q \rangle \geqslant 0$, contour intervals – ± 0.05, ± 0.1, ± 0.2, ± 0.4, ± 0.8.

significant one at the same streamwise section as the centre but on the opposite side of the cylinder centreline, e.g. in phase 7 at $(x, y) \approx (6, 3)$. The major difference in the $\langle q \rangle$-distribution between one- and two-cylinder results lies primarily in the peak magnitudes. Values of $\langle q \rangle$-minima for the one-cylinder case are comparable to those of outer structures, but are noticeably larger than those of inner structures. In contrast, the high-$\langle s \rangle$ region at $(x, y) \approx (4.1, 0)$ in phase 3, which is associated with an inner structure, exhibits a higher peak $\langle q \rangle$ than the corresponding feature in the one-cylinder case, or than the corresponding feature of the outer structure in the two-cylinder case.

High strain rates rather than large Reynolds stresses have been suggested as

being primarily responsible for turbulence production (e.g. Cantwell & Coles 1983). A strong correlation between positive $\langle q \rangle$ and $\langle P \rangle$ might therefore be expected, and high-$\langle P \rangle$ and high-$\langle q \rangle$ regions on the centreline do coincide with each other. Nevertheless, while high-$\langle P \rangle$ and high-$\langle q \rangle$ regions frequently overlap, some notable exceptions may be found, such as the 'outer' high-$\langle q \rangle$ region in phase 7 towards the free stream at $(x, y) \approx (4.7, 2.5)$, or in the one-cylinder case, the outer high-$\langle q \rangle$ region at $(x, y) \approx (3.6, 0.3)$, which both do not exhibit high $\langle P \rangle$. High strain rates alone do not necessarily result in high $\langle P \rangle$; in the two-cylinder case, the high $\langle q \rangle$ on the centreline is complemented by high $[\langle v'^2 \rangle - \langle u'^2 \rangle]$ ($\langle P \rangle = [\langle v'^2 \rangle - \langle u'^2 \rangle]\langle q \rangle^{1/2}$ on $y = 0$).

4.10. *Critical points*

Critical points, namely stationary points in a reference frame moving with the vortex structure, have also been used to describe essential flow features (Cantwell & Coles 1983; Chong *et al.* 1990). In a two-dimensional flow, they appear as centres, associated with closed streamlines, or as saddles, associated with converging and diverging streamlines. The sign of $\langle q \rangle$ at a critical point determines its nature, for $\langle q \rangle < 0$ indicates a centre, i.e. a locally elliptic region associated with circular motion, whereas $\langle q \rangle > 0$ indicates a saddle, i.e. a locally hyperbolic region associated with converging and diverging flows. Alternatively, centres and saddles can be directly interpreted as extrema and saddle points of the phase-averaged stream function, $\langle \psi \rangle$, in which case $\langle q \rangle = \langle \psi \rangle_{xy}^2 - \langle \psi \rangle_{xx}\langle \psi \rangle_{yy}$ can be related to the curvature of $\langle \psi \rangle$. Since $\langle q \rangle < 0$ (or $\langle q \rangle > 0$) may be satisfied at points other than critical points, the classification of critical points can only proceed after their location has been identified by other procedures. Though more sophisticated identification techniques have been proposed (Zhou & Antonia 1994), the present work relied on simple visual inspection of streamline plots such as figure 9. The associated uncertainties and possible three-dimensional effects should not significantly affect the following qualitative discussion, but should be borne in mind.

A composite schematic diagram of the flow topologies for the one- and the two-cylinder cases has been constructed in figure 23. Centres in both cases share the same characteristics of high $\langle \omega \rangle$ and high $\langle k \rangle$, but $\langle P \rangle$ may be more significant than generally thought. The two cases differ principally in that two inner saddle points instead of one are required by symmetry about the centreline. The characteristics of outer saddles, i.e. saddles located towards the free stream, are similar to those of one-cylinder saddles. Regions of significant $\langle -u'v' \rangle$ are oriented along the separatrix, but regions of significant $\langle P \rangle$ are more oriented along a line joining centre and saddle. In contrast, the two inner saddles, located along the centreline, must by symmetry exhibit negligible $\langle -u'v' \rangle$. Since the saddles are formed by the streamline separatrix around a structure, the saddles are labelled with a superscript indicating the 'associated' structure. Thus, the outer saddle, s^A, is associated in this way with the inner structure, A. The two inner saddles, labelled s_u^B and s_d^B, are located upstream and downstream of the outer structure, B.

The relationship between a saddle and the 'associated' structure is weak. The inner structure is strongly affected by the presence of the other cylinder, but it is 'associated' with an outer saddle that is negligibly affected by interactions across the centreline. Similarly, outer-structure saddles have been qualitatively affected, but outer-structure characteristics are relatively unchanged from those of one-cylinder structures. As the discussion of figure 13 and figure 16 noted, the $\tilde{u}\tilde{u}_p$- and $\langle -u'v' \rangle$-distributions are also only loosely related, if at all, to the structure in their immediate vicinity. This raises

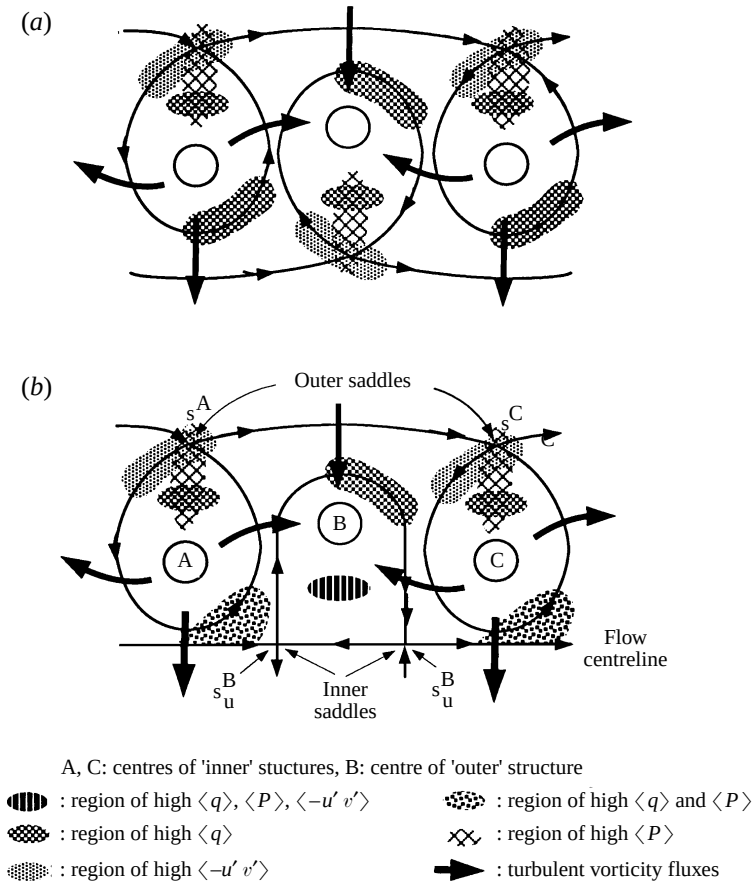

FIGURE 23. Schematic diagram of flow topologies of (*a*) the one-cylinder case, and (*b*) the two-cylinder case.

the question of whether this association, based on a streamline geometry, between saddle and structure is useful and if not whether the concept of a saddle or the relationship between saddle and structure should be modified.

From a topological point of view, inner and outer saddles are identical, and so should share similar kinematic features, but quantitative differences between inner and outer saddles, and even between the two inner saddles, are apparent. Significant though not necessarily local peak values of $\langle q \rangle$ are observed in saddle regions. LERP had already noted that, in the one-cylinder case, the largest strain rates and hence $\langle q \rangle$ were observed away from saddles. The upstream inner saddle, (s_u^B in figure 23), is associated with noticeably larger $\langle q \rangle$ than that of the other inner saddle (figure 22), but this is not necessarily the case when $\langle P \rangle$ is considered (figure 21). The peak value of $\langle q \rangle$ occurs upstream of s_u^B, and is larger than the corresponding peak near the outer saddle. The increased value may be understood in terms of the shorter streamwise lengthscales caused by an upstream displacement of the saddle, leading to larger gradients. The larger streamwise lengthscales between the two inner saddles, together with the damping of cross-stream motion, contribute to the disparity of $\langle q \rangle$ between the two inner saddles. The behaviour of the $\langle P \rangle$-distribution in the centreline region is more complicated, since it depends also on the turbulence field, particularly,

$[\langle v'^2\rangle - \langle u'^2\rangle]$. Figure 20 shows that $[\langle v'^2\rangle - \langle u'^2\rangle]$ is large and positive around s_u^B, where $\langle u\rangle_x > 0$, and is negative around s_d^B, where $\langle u\rangle_x < 0$, resulting in positive $\langle P\rangle$ of, however, variable magnitude. An alternative viewpoint sees the splitting of the one-cylinder saddle into two inner saddles as being reflected in a splitting of $\langle P\rangle$- and $\langle q\rangle$-distributions (figures 21 and 22) compared to the one-cylinder distributions. A direct effect of the split saddles on the $\langle k\rangle$- and $\langle -u'v'\rangle$-distributions, if there is any, is more difficult to discern.

5. Summary

The unsteady flow around two identical square-sectioned cylinders placed side by side was studied using laser-Doppler velocimetry and ensemble averaging. Measurements were made for a Reynolds number of 23 100 and a gap/diameter ratio of 2. A coupled vortex street, in a predominantly in-antiphase mode where the flow is symmetric about the centreline, resulted. The time-averaged velocity field showed a jet flow in the gap, which eventually develops into a more wake-like flow. Differences from the time-averaged one-cylinder flow were surprisingly small in the measurement region. The phase-averaged fields showed, however, a marked quantitative difference between the streamwise evolution of vortex structures shed towards the free stream and those shed towards the centreline. The former (outer) structure was practically unaffected by the presence of the second cylinder, but the vorticity and circulation of the inner structure were sharply reduced in the near wake. The inequality of the circulation of inner and outer structures supports the theoretical conclusions of Landweber (1942). The apparent conflict between the Landweber predictions and arguments by Bearman & Wadcock (1973) based on pressure measurements on the cylinder surface was resolved by noting that the Landweber theory applied only away from the cylinder, while the Bearman & Wadcock argument applied only to the immediate vicinity of the cylinder.

The Strouhal number was found to be slightly higher than that observed in the one-cylinder case (0.14 compared to 0.13), while previous work suggests that the Strouhal numbers are the same in both cases. The symmetry constraint on the centreline promotes streamwise motion while inhibiting cross-stream motion, thus leading to shorter streamwise lengthscales, and this may lead to a slightly higher vortex shedding frequency. Owing to the enhanced streamwise motion, the average vortex speed in the base region is significantly higher for the two-cylinder case, though in the eventual near-wake 'equilibrium' state, the vortex speed is slightly smaller. The centreline constraint also forces the structures as they grow in size to move farther away from the centreline, but this is compensated by the inhibition of cross-stream motion, such that the width of the wake (measured from the cylinder centreline) may not be significantly changed.

The distribution of turbulence characteristics differs most notably from the one-cylinder case in the region of the centreline, with significantly higher turbulent kinetic energy but smaller Reynolds shear stress. In spite of negligible Reynolds shear stress along the centreline, vorticity could be exchanged across the centreline by non-zero gradients of Reynolds stresses. This was argued to be the main cause of the striking changes in circulation of the inner structure. The relationships between turbulence production, the invariant obtained from the velocity gradient tensor, and critical points were also examined. A one-to-one relationship between large strain rates and high turbulence production was not found, pointing to the importance of Reynolds stresses for the latter. As in the one-cylinder case, centres were characterized by

vorticity extrema, minima in the characteristic discriminant, peak turbulent kinetic energies, and often significant turbulence production, but these were not strongly related to the region of high Reynolds shear stresses in the vicinity of the centre. Saddles were more problematic to characterize consistently. Outer saddles, located towards the free stream, were similar to one-cylinder saddles with generally high turbulence production and Reynolds shear stresses. Inner saddles, located on the centreline, were necessarily regions of negligible Reynolds shear stress, but were often located in the neighbourhood of significant strain rates and turbulence production.

The experimental work was performed at the Institut für Hydromechanik, Universität Karlsruhe, and was financially supported by the German Research Foundation through the Sonderforschungsbereich 210. The first author also gratefully acknowledges the support of the Alexander von Humboldt Foundation and of the GA Academy of Sciences, Czech Republic, through grant A260403. The experimental rig was constructed by Mr D. Bierwirth.

Appendix. Vorticity fluxes

For flows of a homogeneous fluid, the phase-averaged vorticity equation may be written in tensor notation as (Tennekes & Lumley, 1972)

$$\frac{\mathrm{D}\langle\Omega_i\rangle}{\mathrm{D}t} = \langle\Omega_j\rangle\langle S_{ij}\rangle + \frac{\partial}{\partial x_j}\left[\langle\Omega'_j u'_i\rangle - \langle u'_j\Omega'_i\rangle\right] + \frac{1}{Re}\frac{\partial^2\langle\Omega_i\rangle}{\partial x_j x_j}, \tag{1}$$

where $\langle S_{ij}\rangle$ is the phased-averaged strain-rate tensor, and the turbulence terms have been written in divergence form. Because the fluctuating velocity field is solenoidal, the turbulent vorticity 'flux' terms can be expressed purely in terms of a second-order tensor of velocity fluctuation correlations as

$$J_{ij} = \langle u'_j\Omega'_i\rangle - \langle\Omega'_j u'_i\rangle = \epsilon_{ijk}\frac{\partial\langle T^*_{lk}\rangle}{\partial x_l}, \tag{2}$$

where $T^*_{ij} \equiv \langle u'_l u'_j\rangle - (\langle u'_l u'_l\rangle/2)\delta_{ij}$, ϵ_{ijk} is the permutation symbol, and δ_{ij} is the Kronecker delta symbol. In this way, the turbulent vorticity flux tensor, J_{ij}, can be directly related to the gradients of the Reynolds stress tensor.

REFERENCES

Basdevant, C. & Philipovitch, T. 1994 On the validity of the "Weiss criterion" in two-dimensional turbulence. *Physica* D **73**, 17–30.

Bearman, P. W. & Wadcock, A. J. 1973 The interaction between a pair of circular cylinders normal to a stream. *J. Fluid Mech.* **61**, 499–511.

Bosch, G. 1995 Experimentelle und theoretische Untersuchung der instationären Strömung um zylindrische Strukturen. PhD thesis, University Karlsruhe, Germany.

Cantwell, B. J. & Coles, D. 1983 An experimental study of entrainment and transport in the turbulent near-wake of a circular cylinder. *J. Fluid Mech.* **135**, 321–374.

Chang, K.-S. & Song, Ch.-J. 1990 Interactive vortex shedding from a pair of circular cylinders in a transverse arrangement. *Intl J. Numer. Meth. Fluids* **11**, 317–329.

Chong, M. S., Perry, A. E. & Cantwell, B. J. 1990 A general classification of three-dimensional flow field. *Phys. Fluids* A **2**, 765–777.

Hayakawa, M. & Hussain, F. 1989 Three-dimensionality of organized structures in a plane turbulent wake. *J. Fluid Mech.* **206**, 375–404.

Hussain, A. K. M. F. 1983 Coherent structures – reality and myth. *Phys. Fluids* **26**, 2816–2850.

Hussain, A. K. M. F. & Hayakawa, M. 1987 Eduction of large-scale organized structures in a turbulent plane wake. *J. Fluid Mech.* **180**, 193–229.

Jeong, J. & Hussain, A. K. M. F. 1995 On the identification of a vortex. *J. Fluid Mech.* **285**, 69–94.

Kim, H. J. & Durbin, P. A. 1988 Investigation of the flow between a pair of circular cylinders in the flopping regime. *J. Fluid Mech.* **196**, 431–448.

Kiya, M. & Matsumara, M. 1988 Incoherent turbulence structure in the near wake of a normal flat plate. *J. Fluid Mech.* **190**, 343–356.

Landweber, L. 1942 Flow about a pair of adjacent, parallel cylinders normal to a stream. *Navy Dept., David W. Taylor Model Basin, Rep.* 485, *July*.

Lighthill, M. J. 1963 Introduction. Real and ideal fluids. In *Laminar Boundary Layers* (ed. L. Rosenhead). Clarendon.

Lyn, D. A., Einav, S., Rodi, W. & Park, J.-H. 1995 A laser-Doppler velocimetry study of ensemble-averaged characteristics of the turbulent near wake of a square cylinder. *J. Fluid Mech.* **304**, 285–320 (referred to herein as LERP).

Lyn, D. A. & Rodi, W. 1994 The flapping separated shear layer formed by flow separation from the forward corner of a square cylinder. *J. Fluid Mech.* **267**, 353–376.

Ng, C. W. & Ko, N. W. M. 1995 Flow interaction behind two circular cylinders of equal diameter – a numerical study. *J. Wind Engng Ind. Aerodyn.* **54/55**, 277–288.

Segel, L. A. 1977 *Mathematics Applied to Continuum Mechanics.* Macmillan.

Spivack, H. M. 1946 Vortex frequency and flow pattern in the wake of a two parallel cylinders at varied spacings normal to an air stream. *J. Aero. Sci.* **13**, 289–297.

Stansby, P. K. 1981 A numerical study of vortex shedding from one and two circular cylinders. *Aero. Q.* **32**, 48–71.

Tennekes, H. & Lumley, J. L. 1972 *A First Course in Turbulence.* MIT Press.

Weiss, J. 1991 The dynamics of enstrophy transfer in two-dimensional hydrodynamics. *Physica* D **48**, 273–294.

Williamson, C. H. K. 1985 Evolution of a single wake behind a pair of bluff bodies. *J. Fluid Mech.* **159**, 1–18.

Wray, A. A. & Hunt, J. C. R. 1990 Algorithms for classification of turbulent structures. In *Topological Fluid Mechanics, Proc. IUTAM Symp. Cambridge*, 1989 (ed. H. K. Moffatt & A. Tsinober), pp. 95–104. Cambridge University Press.

Zdravkovich, M. M. 1977 Review of flow interference between two circular cylinders in various arrangements. *Trans. ASME: J. Fluids Engng* **99**, 618–633.

Zhou, Y. & Antonia, R. A. 1994 Critical points in a turbulent near wake. *J. Fluid Mech.* **275**, 59–81.